

Prediction of earthquake ground motion at rock sites in Japan: evaluation of empirical and stochastic approaches for the PEGASOS Refinement Project

Journal Article**Author(s):**

Edwards, Benjamin; Fäh, Donat

Publication date:

2017-11

Permanent link:

<https://doi.org/10.3929/ethz-b-000219975>

Rights / license:

[In Copyright - Non-Commercial Use Permitted](#)

Originally published in:

Geophysical Journal International 211(2), <https://doi.org/10.1093/gji/ggx328>

Prediction of earthquake ground motion at rock sites in Japan: evaluation of empirical and stochastic approaches for the PEGASOS Refinement Project

Benjamin Edwards¹ and Donat Fäh²

¹Department of Earth, Ocean and Ecological Sciences, University of Liverpool, Liverpool L69 3GP, United Kingdom. E-mail: ben.edwards@liverpool.ac.uk

²Swiss Seismological Service, ETH Zürich, Sonneggstrasse 5, CH-8092 Zurich, Switzerland

Accepted 2017 August 2. Received 2017 June 22; in original form 2016 December 1

SUMMARY

Strong ground-motion databases used to develop ground-motion prediction equations (GMPEs) and calibrate stochastic simulation models generally include relatively few recordings on what can be considered as engineering rock or hard rock. Ground-motion predictions for such sites are therefore susceptible to uncertainty and bias, which can then propagate into site-specific hazard and risk estimates. In order to explore this issue we present a study investigating the prediction of ground motion at rock sites in Japan, where a wide range of recording-site types (from soil to very hard rock) are available for analysis. We employ two approaches: empirical GMPEs and stochastic simulations. The study is undertaken in the context of the PEGASOS Refinement Project (PRP), a Senior Seismic Hazard Analysis Committee (SSHAC) Level 4 probabilistic seismic hazard analysis of Swiss nuclear power plants, commissioned by *swissnuclear* and running from 2008 to 2013. In order to reduce the impact of site-to-site variability and expand the available data set for rock and hard-rock sites we adjusted Japanese ground-motion data (recorded at sites with $110 \text{ m s}^{-1} < V_{S30} < 2100 \text{ m s}^{-1}$) to a common hard-rock reference. This was done through deconvolution of: (i) empirically derived amplification functions and (ii) the theoretical 1-D *SH* amplification between the bedrock and surface. Initial comparison of a Japanese GMPE's predictions with data recorded at rock and hard-rock sites showed systematic overestimation of ground motion. A further investigation of five global GMPEs' prediction residuals as a function of quarter-wavelength velocity showed that they all presented systematic misfit trends, leading to overestimation of median ground motions at rock and hard-rock sites in Japan. In an alternative approach, a stochastic simulation method was tested, allowing the direct incorporation of site-specific Fourier amplification information in forward simulations. We use an adjusted version of the model developed for Switzerland during the PRP. The median simulation prediction at true rock and hard-rock sites ($V_{S30} > 800 \text{ m s}^{-1}$) was found to be comparable (within expected levels of epistemic uncertainty) to predictions using an empirical GMPE, with reduced residual misfit. As expected, due to including site-specific information in the simulations, the reduction in misfit could be isolated to a reduction in the site-related within-event uncertainty. The results of this study support the use of finite or pseudo-finite fault stochastic simulation methods in estimating strong ground motions in regions of weak and moderate seismicity, such as central and northern Europe. Furthermore, it indicates that weak-motion data has the potential to allow estimation of between- and within-site variability in ground motion, which is a critical issue in site-specific seismic hazard analysis, particularly for safety critical structures.

Key words: Earthquake ground motions; Earthquake hazards; Seismic attenuation; Site effects.

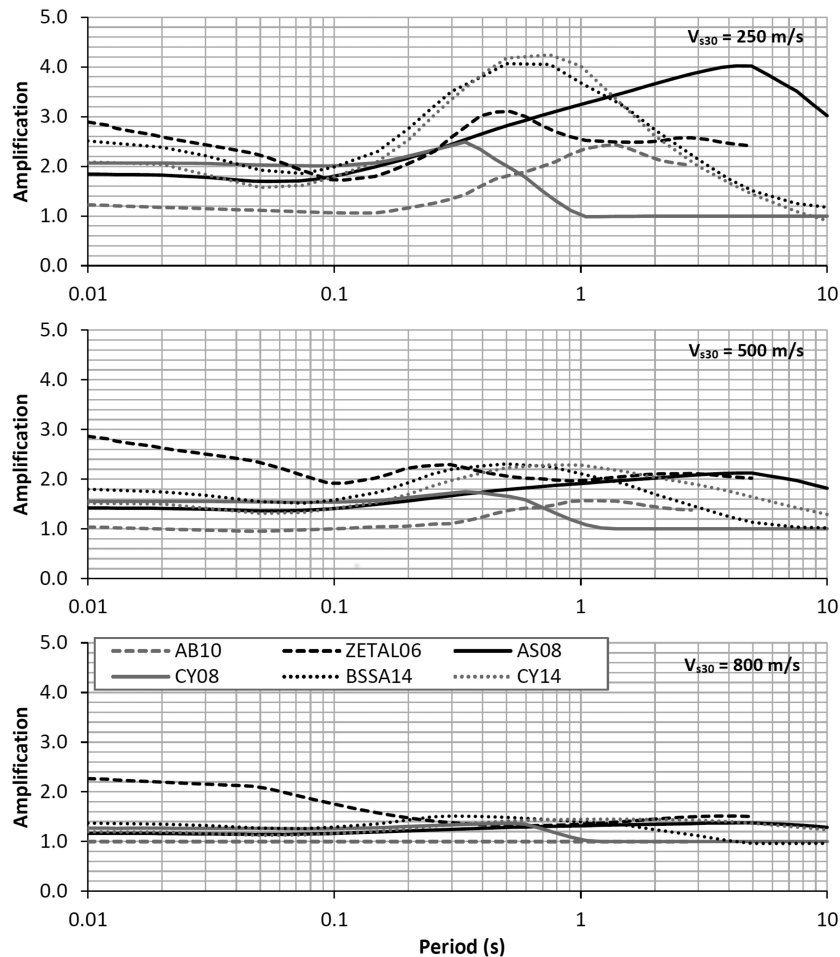


Figure 1. Amplification of 5 per cent damped PSA according to six GMPEs. Amplification is calculated relative to their predictions at $V_{S30} = 1350 \text{ m s}^{-1}$ for: $V_{S30} = 800 \text{ m s}^{-1}$ (bottom); $V_{S30} = 500 \text{ m s}^{-1}$ (middle); and $V_{S30} = 250 \text{ m s}^{-1}$ (top panel). Predictions are for a surface rupture $M = 6$ event at $R_{JB} = 50 \text{ km}$. AB10 (Akkar & Bommer 2010); ZETAL06 (Zhao *et al.* 2006); AS08 (Abrahamson & Silva 2008); CY08 (Chiou & Youngs 2008); BSSA14 (Boore *et al.* 2014); CY14 (Chiou & Youngs 2014).

1 INTRODUCTION

The estimation of expected ground motion for scenario earthquakes in seismic hazard studies is typically performed using ground-motion prediction equations (GMPEs), which are based on empirical strong ground-motion data (Douglas & Edwards 2016). For example, the Next Generation Attenuation (NGA) West-1 and -2 data sets (Chiou *et al.* 2008; Ancheta *et al.* 2014) and associated models (e.g. Abrahamson *et al.* 2008); the European and Middle-East data sets, such as RESORCE (Akkar *et al.* 2014) and associated models (Douglas *et al.* 2014); and other global and regional models (e.g. Bindi *et al.* 2011; Laurendeau *et al.* 2013; Cauzzi *et al.* 2015; Drouet & Cotton 2015). Users provide a number of descriptive parameters of an earthquake scenario to obtain the expected ground motion and its uncertainty in terms of the peak response of a damped single-degree-of-freedom oscillator. This approach is appropriate when target scenarios are within the data-space used for the derivation of the model. Limitations arise, however, as with any inverse-problem, when we wish to apply the models in parameter-space that is poorly represented by the original data set. GMPEs are the least robust at the edge of their model space due to a lack of data (e.g. Zhao & Lu 2011), which leads to potential model bias, driven partly by available

data, and partly modelling decisions. For instance, results in data-poor model space may be driven by choices of model form (e.g. V_{S30} based amplification, near source saturation or magnitude scaling) or simulations. Ground-motion amplification predicted by GMPEs is therefore potentially not robust for less-commonly occurring site types such as those with very soft (nonlinear) soils, or hard rock. An example can be observed by comparing amplification predicted by different GMPEs at V_{S30} values of 800, 500 and 250 m s^{-1} with respect to the same GMPEs' predictions at a reference rock-site ($V_{S30} = 1350 \text{ m s}^{-1}$) (Fig. 1). Differences in amplification between six selected models, even between those using the same NGA data set [Chiou & Youngs (2008) and Abrahamson & Silva (2008)] reach up to a factor of four. This is consistent with the observations of Poggi *et al.* (2017), who found that GMPEs were not able to accurately represent site amplification, although recent NGA-West2 models (e.g. Boore *et al.* 2014; Chiou & Youngs 2014) appear to provide more consistent results (Fig. 1). As a result of this non-uniqueness a significant limitation arises when we wish to adjust GMPEs for target-specific site characteristics, such as in the case of a site-specific hazard study (e.g. for a nuclear power facility or hydroelectric dam) or when developing regional hazard maps referenced to a local velocity profile.

2 SITE SPECIFIC GROUND MOTION IN CURRENT PRACTICE

For single-site hazard analyses ground motion is typically predicted at a reference rock or hard rock [e.g. bedrock or reference rock model (Boore & Joyner 1997; Poggi *et al.* 2011; Hashash *et al.* 2014)]. Subsequent site-specific anelastic amplification is then applied to obtain the ground motion and related hazard at the surface. In this way, site amplification is effectively decoupled from the prediction allowing more thorough consideration of a site's response to ground motion, including factors such as resonance, nonlinearity and uncertainties. High V_s ground-motion predictions are, therefore, critical in modern PSHA. Ideally a high V_s reference should be chosen (i.e. below which can be assumed a half-space), however as discussed previously, observations at sites with increasingly high shear-wave velocities are relatively sparse, particularly for larger near-field events—GMPEs therefore rely on extrapolation outside the well-sampled data-space. This may lead to predictions that are not robust or potentially biased.

In order to overcome the high- V_s limitation, GMPEs may be used to predict ground motions at sites where they are considered robust (e.g. on stiff soil, $500 < V_{S30} < 800 \text{ m s}^{-1}$ sites; known as the host) with a subsequent physically based adjustment (accounting for uncertainties) to convert to a target hard-rock site (e.g. Renault 2014; Edwards *et al.* 2016). A limitation of GMPE adjustment, however, is that they must first be converted to equivalent Fourier models. To achieve this, minimum misfit Fourier Acceleration spectrum (FAS) based models (Campbell 2003; Scherbaum *et al.* 2006) or response spectra consistent FAS (Al Atik *et al.* 2014) can be calculated. Due to the simplified basis of empirical response spectra based models, any physically-based adjustment (e.g. for different site amplification) is inherently complicated. The adjustment approaches are highly non-unique and nonlinear, not least due to the fact that a significant amount of short-period ground-motion information is irretrievable from response spectra upon which GMPEs are based (Kottke & Rathje 2008; Bora *et al.* 2016).

Instead of relying on empirical models, an alternative approach to ground-motion prediction is to use models based directly on Fourier Acceleration Spectra (FAS) and shaking-duration. These models relate the FAS and duration of shaking through stochastic simulation (Boore 2003; Motazedian & Atkinson 2005) or random-vibration theory (RVT; Atkinson & Boore 2006; Edwards & Fäh 2013; Drouet & Cotton 2015; Bommer *et al.* 2017). Such models are calibrated based on physical properties of earthquake source processes, attenuation, and site amplification. These phenomena are typically modelled or measured from recordings of earthquakes in the target region (e.g. Edwards *et al.* 2008; Drouet *et al.* 2011; Bommer *et al.* 2016). The advantage of this is that the resulting ground-motion prediction is based on data from the study region, and should therefore include any associated features of source physics, wave propagation and site-specific effects.

FAS based models (e.g. stochastic simulation models) are implicitly easier to adjust than empirical GMPEs (Bora *et al.* 2013) and can be linked to physical processes (Baltay *et al.* 2017). For instance, FAS can easily be adjusted to a specific site using V_s and density profiles and associated anelastic amplification (Poggi *et al.* 2013). Epistemic uncertainty may also be easier to quantify, since physically interpretable parametric variability (e.g. stress-drop, attenuation and site amplification) can be given as distributions rather than a unique value. On the other hand, with simulation approaches we still rely on assumptions and broad simplifications in order to extend the predictions to earthquakes of engineering interest, albeit with scope for physical reasoning behind the extrapolation.

In the following sections we present the results of a study exploring the prediction of ground motion at rock sites which was carried in light of the difficulties observed adjusting empirical GMPEs during the PEGASOS Refinement Project (PRP; Renault 2014). We test the performance of different empirical (GMPE) and stochastic simulation approaches used in the project in order to predict strong ground motion at instrumented sites in Japan. GMPE model choice was primarily based on models used in the PRP. However, in order to broaden the applicability of the results we have extended the analysis to an additional NGA-West2 GMPE. We test the ability of the methods to predict ground motion at reference rock or bedrock velocities. In both cases, we predict ground motion over the complete database of recordings, including soil and soft-soil sites. We then make a subselection of sites based on either V_{S30} or amplification behaviour in order to assess the performance at rock sites. We finally adjust the Swiss FAS based (stochastic simulation) model developed for the PRP, in order to predict ground motion in Japan, and test the predictions against the same data set.

3 GROUND-MOTION DATA SET

We use data from surface accelerometers of the Japanese free-field strong motion network KiK-Net (Aoi *et al.* 2004). Each station of the network has a corresponding shear-wave velocity profile down to the depth of a co-located borehole accelerometer and high-gain seismometer (100–200 m, depending on site). The shear-wave velocity profiles are based on PS logging and are provided by the NIED (www.kyoshin.bosai.go.jp). The downhole instruments are not used in this study. All events used are crustal earthquakes (depth less than 25 km) and have magnitudes $M > 5$. The time-series data are initially checked using a signal-to-noise ratio (SNR) analysis. Using this information, the time-series are padded and band-pass filtered [6-pole acausal butterworth, (Boore 2005)] in order to retain the signal over a continuous bandwidth with SNR greater than 3. The resulting traces are then used to compute the 5 per cent damped pseudo-spectral acceleration (PSA) response spectra following the method of Nigam & Jennings (1969). We only analyse response spectra at periods less than $0.8T_{\max}$ to avoid the effect of the long-period cut-off filter, where T_{\max} is the corner-period of the filter (Akkar & Bommer 2006). As a result of the shape of earthquake source acceleration spectra for moderate-to-large events and the effect of attenuation, periods of the response spectrum greater than the short-period cut-off filter are still useful due to the sensitivity of high-frequency oscillators to lower-frequency ground motion (Douglas & Boore 2011). The range of valid periods therefore spans PGA to $0.8T_{\max}$.

The frequency range of waveform FAS with acceptable SNR, and magnitude and distance coverage of the database is shown in Fig. 2. Minimum frequencies of lower than 0.1 Hz are typical, while upper Fourier spectral frequencies are available to 30 Hz [this maximum frequency is defined by a low-pass filter applied to the data by the Japanese National Research Institute for Earth Science and Disaster Prevention, NEID (Aoi *et al.* 2004)]. As expected, due to the lower damping (κ_0), the recordings at rock and hard-rock sites ($V_{S30} > 800 \text{ m s}^{-1}$) exhibit a significantly higher proportion of high-frequency motions above the noise level. The maximum event magnitude in our database was $M_W = 7.4$ (although only sparsely recorded at rock sites). A fairly uniform distribution of distance and depth for events with magnitudes in the range $5.3 < M < 7$ is available. Unfortunately, however, rock site recordings were not available for the largest event at distances less than 200 km. We note here that while the band-limited

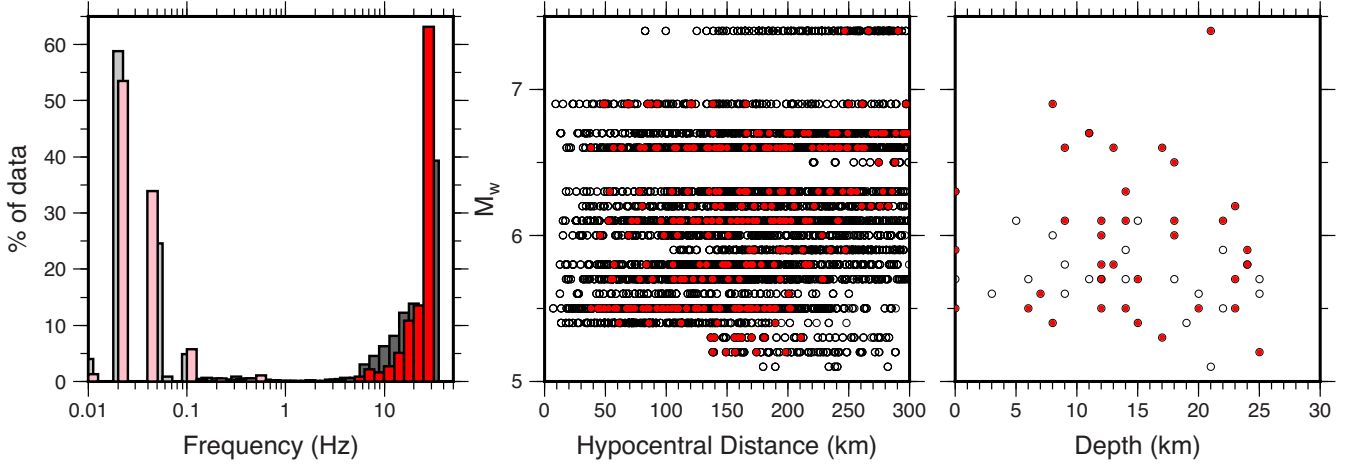


Figure 2. Data available for this analysis (grey/black: all sites; red: sites with $V_{S30} > 800 \text{ m s}^{-1}$). Left: high-pass (light shade) and low-pass (dark shade) frequencies of the SNR analysis (i.e. $\text{SNR} > 3$ within the limits). Middle: hypocentral distance versus magnitude; right: hypocentral depth versus magnitude.

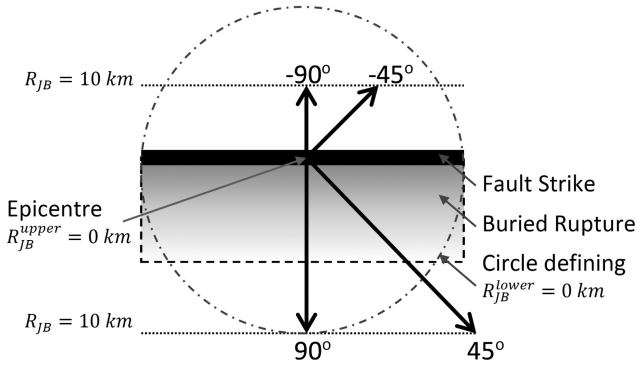


Figure 3. Aerial view of fault and simulation directions. The circle indicates the zone over which we assume zero R_{JB}^{lower} distance: the area where it is possible the surface projection of the fault strike exists.

recordings ($f < 30 \text{ Hz}$) could theoretically prevent the observation of very high-frequency PSA amplification effects, this would only be apparent for very near-field recordings due to the effect of Q and κ and the sensitivity of PSA to different oscillator periods (Bora *et al.* 2016).

Since fault-orientation and distance-metrics were not available for all events, we estimated all distances in terms of (a) a lower-bound (R_{JB}^{lower}) and (b) an upper-bound estimate (R_{JB}^{upper}) of the distance to the fault surface-projection using:

$$R_{JB}^{\text{lower}} = \max\left(\sqrt{(R_h^2 - H^2)} - \frac{L}{2}, 0\right) \quad (1)$$

$$R_{JB}^{\text{upper}} = R_{\text{epi}} = \sqrt{(R_h^2 - H^2)} \quad (2)$$

where L is the fault length and H is source depth, assuming a strike-slip mechanism and the relations of Wells & Coppersmith (1994), and R_h is the hypocentral distance. The upper bound is equivalent to the epicentral distance. For the lower bound we define an estimate of the surface projection of the fault (where $R_{JB} = 0$). This is equivalent to rotating the fault strike through 360° around the epicentre to draw a circle with diameter equal to the length of the fault (Fig. 3). We average predictions over a range of source-receiver paths ($-90^\circ, -45^\circ, 0^\circ, 45^\circ$ and 90°) to account for unknown strikes (Fig. 3).

Depth to the top of the fault was approximated as:

$$Z_{\text{top}} = H - \frac{W}{2} \sin\left(\frac{79\pi}{180}\right) \quad (3)$$

with W the fault width for a strike slip event (with dip 79°) for a given magnitude from Wells & Coppersmith (1994). Finally, the rupture distance was estimated using

$$R_{\text{rup}}^{\text{lower|upper}} \approx \sqrt{(R_{JB}^{\text{lower|upper}})^2 + Z_{\text{top}}^2} \quad (4)$$

with superscripts ‘lower’ or ‘upper’ signifying the use of the corresponding R_{JB} estimate. We compare the recordings using the relevant site-class predictions (based on V_{S30}) for strike-slip events. All predictions are made at the relevant R_{JB}^{lower} and R_{JB}^{upper} distance measures (with metric dependent on the GMPE), with the range of predictions shown in Fig. 4. Within these limits the possible distribution of the converted distances can be described by a Gamma distribution (Scherbaum *et al.* 2004), which itself can be approximated by a log-normal distribution. Since we plot the residual misfit on log axes, we therefore assume that the mean estimate lies half way between the predictions for the upper and lower distance measures.

4 GMPE PREDICTIONS

In an initial analysis we compare 5 per cent damped pseudo-spectral acceleration spectra data from all site types with predictions from the GMPE of Zhao *et al.* (2006, hereinafter ZETAL06). ZETAL06 is based on Japanese data and has been implemented in various world-wide hazard studies [e.g. Seismic Harmonization in Europe (SHARE, Delavaud *et al.* 2012a), PEGASOS Refinement Project (PRP, Renault 2014), Global Earthquake Model (GEM; Pagani *et al.* 2014)]. Of the available PRP models, this was therefore considered as most applicable to our Japanese data set. In the ZETAL06 model, site class was defined based on the observed resonance frequency at the site, as defined by (Molas & Yamazaki 1995): with rock sites exhibiting fundamental resonance at $T < 0.2 \text{ s}$; stiff-soil sites at $0.2 \text{ s} \leq T < 0.4 \text{ s}$; medium-soil at $0.4 \text{ s} \leq T < 0.6 \text{ s}$; and soft-soil at $T \geq 0.6 \text{ s}$. Equivalent definitions according to V_{S30} were also ‘calculated from site period’ (Zhao *et al.* 2006) with: rock sites having $V_{S30} > 600 \text{ m s}^{-1}$; stiff-soil $300 \text{ m s}^{-1} < V_{S30} \leq 600 \text{ m s}^{-1}$; medium soil $200 \text{ m s}^{-1} < V_{S30} \leq 300 \text{ m s}^{-1}$; soft soil $V_{S30} \leq 200 \text{ m s}^{-1}$. An additional category was defined by Zhao *et al.* for ‘hard

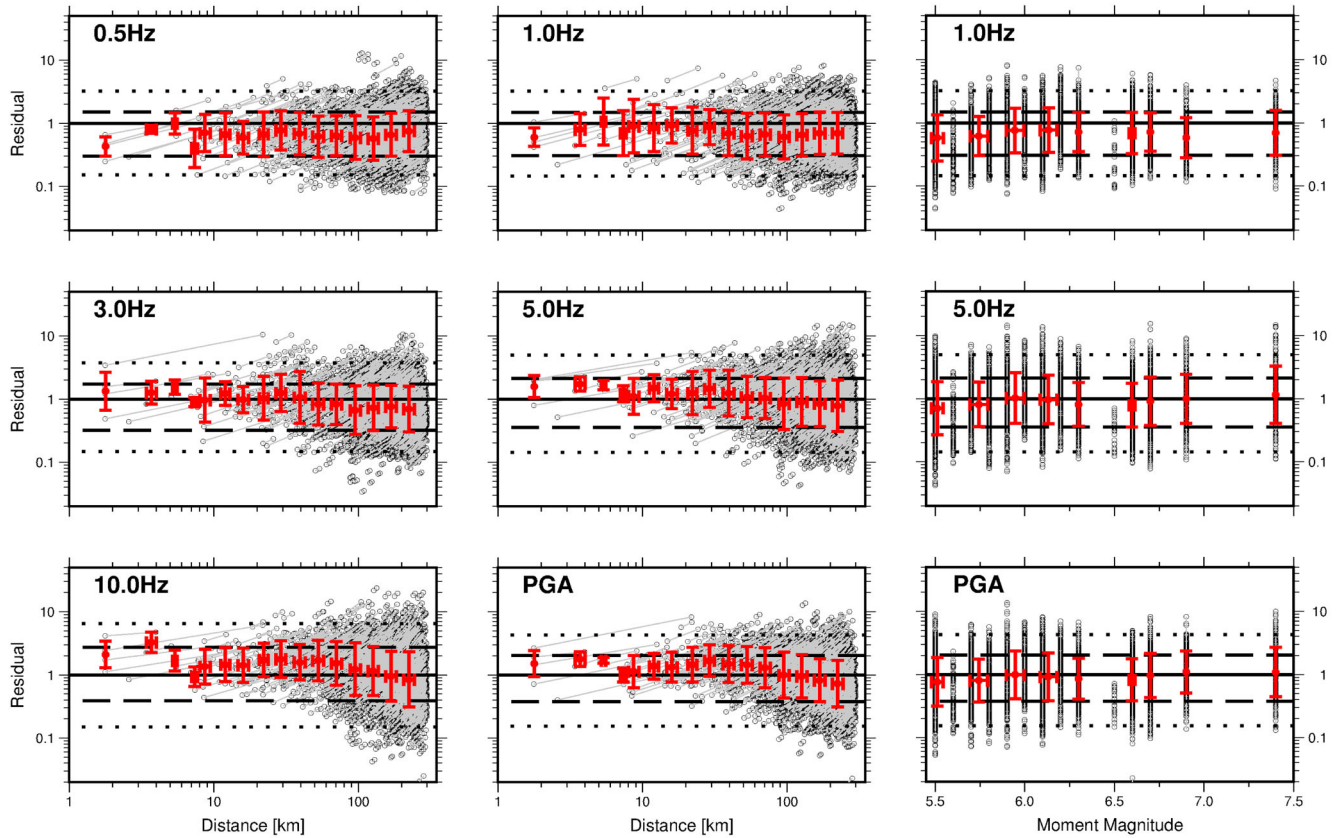


Figure 4. Total misfit (data/model) using the GMPE of Zhao *et al.* (2006) versus rupture distance (left) and magnitude (right) for all site types. The predictions are made for a strike-slip event with site specific V_{S30} values used to determine the relevant site classes. Lines between circles join the GMPE predictions using the estimated lower and uppermost distances (R_{rup}^{lower} and R_{rup}^{upper}) for a single recording. The dashed horizontal lines indicate the average distribution of 68 per cent of the data (approx. one standard deviation), the dotted lines 95 per cent (approx. two standard deviations). Error bars indicate mean and one standard deviation of data within discrete bins.

rock' with $V_{S30} > 1100 \text{ m s}^{-1}$. The latter definitions, using V_{S30} , are more commonly applied, since fundamental periods are often not easily available. The GMPE predictions for our data set are made at the lower and upper bound of R_{rup} for a strike-slip fault. V_{S30} is used to define the relevant site class for use directly in the GMPE. The complete misfit (data/GMPE) is shown in Fig. 4. Note that we do not present a global misfit measure (such as LLH (Scherbaum *et al.* 2009)) as we aim to focus on the detail of the model's residual misfit behaviour, rather than assessing the overall fit.

In an alternative approach to assess the performance of the GMPE, the data are corrected for amplification effects (the specific elastic 1-D *SH* amplification calculated from the site's V_s and density profile), which is compared with a representative 'hard-rock' prediction by the GMPE (Fig. 5). In this case, the misfit is also presented in terms of intra- (within-) and inter- (between-) event terms, which avoids bias due to events with numerous recordings.

Generally, the median prediction (representing the average over all site types) of ZETAL06 performs satisfactorily over the range of spectral ordinates PGA – 0.5 Hz, with the model prediction lying within one standard deviation of the data distribution, and exhibiting no strong bias in magnitude. Systematic biases exist however. At lower frequencies e.g. (0.5 and 1 Hz), the model tends to over-predict (by greater than 50 per cent) the average ground motion over all events. However, looking at the residuals split into inter- and intra-event terms (Fig. 5), we can see that this may be due to the fact that some events (which are overpredicted) contribute more

data than others. ZETAL06 also seems to attenuate somewhat less strongly than the data indicates at higher frequencies ($f > 5 \text{ Hz}$) and distances greater than 100 km, a feature that is present both in total- (Fig. 4) and intra-event residuals (Fig. 5). We note that the GMPE was developed using data recorded at distances up to 300 km, so should be valid in this range. The standard deviation of residual misfit between our data set and the ZETAL06 model (σ_T) is generally higher than published for the original model (e.g. 18 per cent higher at PGA). This may partly be due to the lack of metadata (such as fault mechanism) for most of the events used. However, σ_T we observe is consistent with that reported by Rodriguez-Marek *et al.* (2011), who determined ground-motion prediction uncertainty using only KiK-Net data, as in this study (as opposed to the mixture of KiK-Net, K-Net and other network data in the ZETAL06 data set).

4.1 Rock and hard-rock ground motion

Following the initial analysis of data from all site types, we next make two subselections of the full waveform data set to limit recordings to those representative of (i) rock and hard-rock sites and (ii) sites lacking significant resonance effects. For rock and hard-rock sites, 44 sites with $V_{S30} > 800 \text{ m s}^{-1}$ [Eurocode-8 Class A, (CEN 2004)] are selected. The intra-event residual misfit when compared to ZETAL06 predictions is presented in Fig. 6(a) and

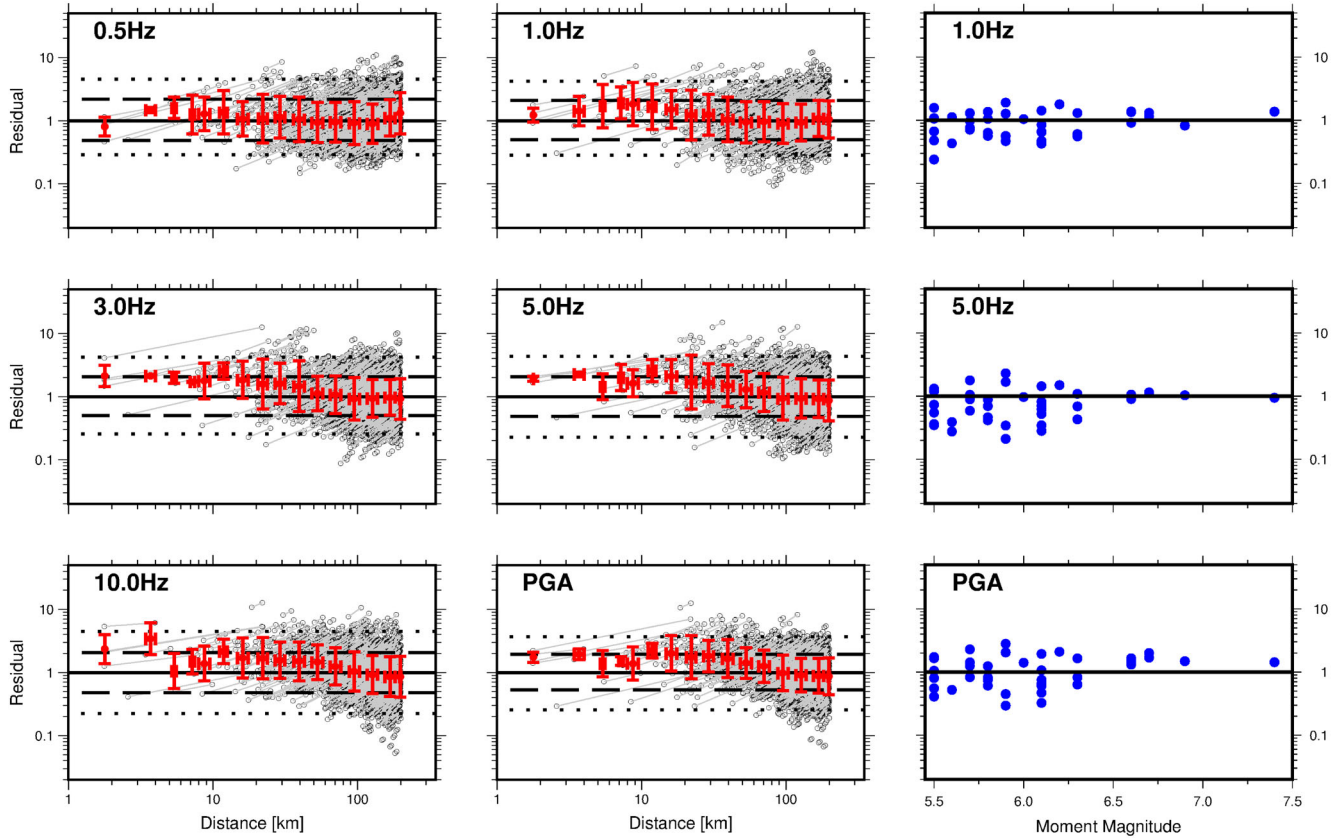


Figure 5. As Fig. 4, but for data ($R_{rup} < 200$ km) at all sites, with data corrected in the Fourier domain to the bedrock using site-specific elastic 1-D SH amplification (all GMPE predictions in this case are made using ZETAL06's 'hard-rock' site class). Left: intra-event residuals; right inter-event residuals.

shows overestimation at low-frequency (1 and 3 Hz) and a distance trend at higher frequencies (≥ 5 Hz). PGA is fitted well 'on average' (the mean misfit data/GMPE is close to unity), but shows a systematic distance trend beyond around 100 km.

In order to account for potential bias due to varying levels of amplification at different sites we then corrected the data for site-specific empirical anelastic site amplification derived using the procedure detailed in Edwards *et al.* (2013). All recorded spectra were therefore effectively corrected to a common Japanese hard-rock velocity profile (Poggi *et al.* 2013) with $V_{S30} = 1350$ m s⁻¹ (Fig. 6b). The average Fourier amplification (site/reference) at some sites is significant, peaking at factors of up to 10 or more at 10–12 Hz. The high levels of amplification are supported by similar values in the surface/borehole spectral ratios computed over the significant duration of shaking. Based on the high resonance frequency this is likely due to a layer of low-velocity weathered material at the surface. After the correction for local amplification effects we observe that the misfit trend with distance in the original PGA data (as seen in Fig. 6a, bottom) is reduced (Fig. 6b, bottom) and may therefore have been an artefact of site-specific amplification. However, the general misfit trends observe in the uncorrected data remain.

Since the correction to the common reference profile involves some interpretation as discussed in Michel *et al.* (2014) and in Poggi *et al.* (2011, 2013), it is possible that bias may lie in the amplification correction, and not the GMPE. To address this we also make use of the theoretical 1-D elastic SH amplification functions corresponding to site-specific velocity profiles provided by the Japanese National Research Institute for Earth Science and

Disaster Prevention (NIED). Correcting the recorded spectra by the SH amplification corresponds to removing the 1-D elastic response of the upper 100–200 m, generally correcting the data to a reference bedrock level, albeit without common velocity. As shown in Fig. 6(c), this leads to a similar result as using the empirical amplification with larger overall scatter of misfit.

4.2 Site selection based on fundamental period

A second subselection of sites was made by taking 59 sites determined by Poggi *et al.* (2013) to show no significant resonance peaks through visual inspection of theoretical 1-D SH amplification and horizontal to vertical (H/V) spectral ratios. A lack of peaks in H/V ratios is due to either being on competent un-weathered rock, or sites with smoothly increasing velocity, lacking any strong velocity contrasts at depth. Despite a larger range of V_{S30} within this selection, it is more consistent with how Zhao *et al.* (2006) defined the site classes, based on geological conditions and the fundamental frequency of resonance (despite also providing a corresponding V_{S30} range which is more commonly used). We nevertheless adopt the site-class term for the GMPE from the site's V_{S30} – since lack of resonance alone does not necessarily indicate a lack of amplification. For this selection the GMPE performs better against the original data across the frequency range, albeit with systematic trends in the residual misfit with distance (Fig. 7a). After correcting the data to the reference profile with $V_{S30} = 1350$ m s⁻¹ (Fig. 7b) or SH amplification to the local bedrock (Fig. 7c), and using the hard-rock GMPE predictions rather than the V_{S30} specific predictions (as per

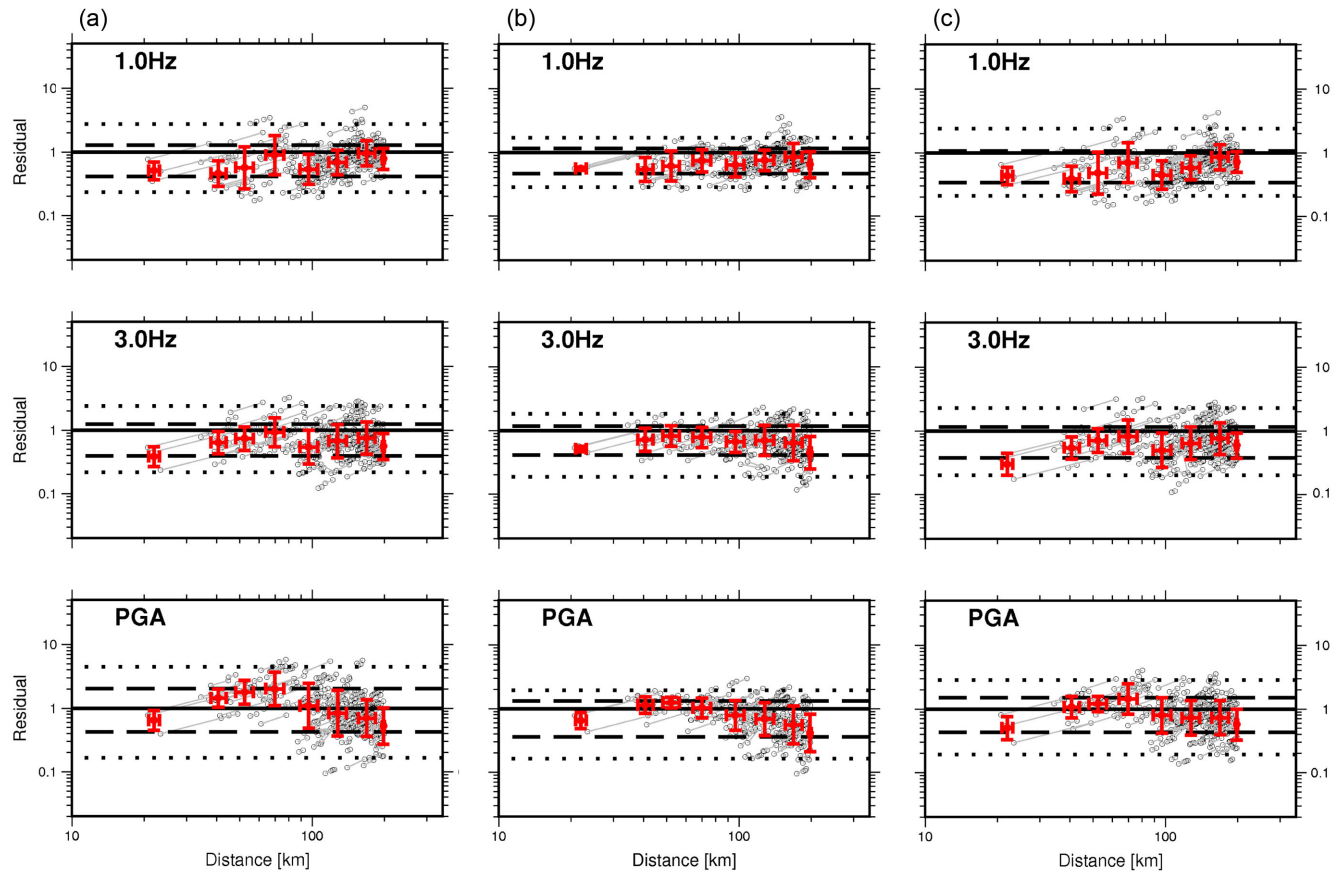


Figure 6. Intra-event misfit (data/model) versus distance for 46 sites with $V_{S30} > 800 \text{ m s}^{-1}$: (a) original spectra (GMPE uses site class based on V_{S30}) (b) data corrected for empirical site amplification to a hard-rock site with $V_{S30} = 1350 \text{ m s}^{-1}$ (GMPE uses hard-rock class, as per ZETAL06's definition); (c) data corrected for elastic SH amplification to the local bedrock (GMPE uses hard-rock class).

Fig. 6), the residual misfit is similar, but in all cases the model tends to underpredict the closest recordings ($R < \sim 50 \text{ km}$).

Initial analyses showed that the GMPE ZETAL06 provides reasonable overall predictions of the ground motions recorded over all surface stations of the KiK-Net accelerograph network (Figs 4 and 5). However, systematic trends are apparent, particularly when making subselections of sites based either on V_{S30} (Fig. 6) or on fundamental period (Fig. 7). The residual behaviour is consistent whether using the GMPE V_{S30} based prediction directly, or correcting data to a common reference rock through deconvolution of empirical or 1-D SH amplification and using the hard-rock class for the GMPE prediction. Importantly for this study, ZETAL06 tends to systematically overpredict motions on KiK-Net rock sites ($V_{S30} > 800 \text{ m s}^{-1}$) (Fig. 6). On the other hand, underprediction tends to be observed at short to moderate distances ($< \sim 50 \text{ km}$) where sites exhibit limited, or no, resonance effects (Fig. 7). The reason behind the under- and overprediction of specific subclasses is not entirely clear. However, it may be due in part to a difference in ‘characteristic site’ for the KiK-Net data we are using. KiK-Net sites are dual borehole-surface installations, with the aim of the borehole being to reach the engineering bedrock within $\sim 100\text{--}200 \text{ m}$ depth (Aoi *et al.* 2004). There are several deeper boreholes, but the majority (~ 88 per cent) are drilled to depths of less than 300 m and 94 per cent are drilled to depths of 500 m or less. Based on this, we assume the sites are less likely to be located on deep ($\sim \text{km}$) sedimentary basins. Resonance phenomena will therefore begin, on average, at higher frequencies on the KiK-Net sites (data used in this study) due

to shallower average bedrock depths. This could explain the overprediction of ZETAL06 with respect to the low- to moderate-period KiK-Net data (Fig. 6). It is, however, not clear why at short distances the GMPE tends to underpredict ground motions for sites lacking resonance, where the opposite would be more intuitive. Nevertheless, this analysis shows that if properly accounting for site-specific amplification effects, the intra-event variability of ground motion has significant potential for reduction—this must, however, be accommodated by improvements in the predictive power of GMPEs or the way in which they are used.

4.3 GMPE misfit as a function of quarter wavelength velocity

A limitation of the GMPE of Zhao *et al.* (2006) is that it did not include a continuous site-specific predictor variable (e.g. V_{S30}). An implicit assumption is therefore that all sites within a given class amplify the ground motion similarly. GMPEs from other authors may be difficult to implement in Japan, since the level of attenuation is relatively strong (Zhao *et al.* 2006). This will lead to biased residuals, which vary as a function of the data's distance distribution. However, assuming that the distance distribution is not correlated with the residuals, we may still look for trends in other parameters after simple corrections are applied (e.g. by increasing the rate of decay with distance).

In order to systematically investigate the dependence of the GMPE predictions on unaccounted site effects, we therefore

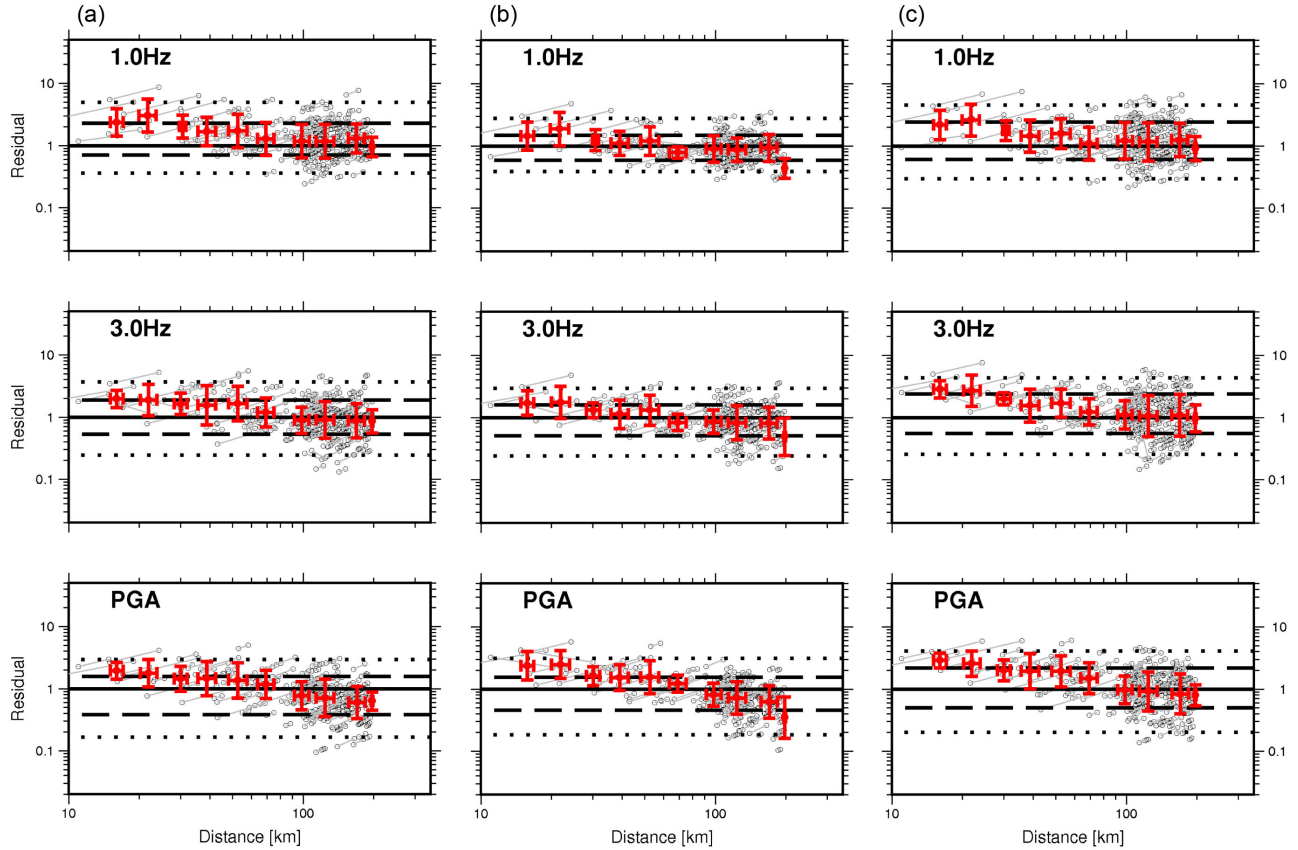


Figure 7. Residual misfit versus distance (as Fig. 4) for 59 sites with no or limited evidence of resonance (Poggi *et al.* 2013) (independent of V_{S30}): (a) original spectra (GMPE uses site class based on V_{S30}) (b) data corrected for anelastic site amplification to a hard-rock site with $V_{S30} = 1350 \text{ m s}^{-1}$ (GMPE uses hard-rock class, as per ZETAL06's definition); (c) data corrected for elastic SH amplification to the local bedrock (GMPE uses hard-rock class).

test their predictions in relation to the sites' quarter-wavelength shear-wave velocities V_S^{QWL} (Joyner *et al.* 1981) using five empirical GMPEs. V_S^{QWL} , like V_{S30} , represents the time-travel average velocity of a given thickness below the surface. However, it extends the idea of V_{S30} by considering the sensitivity of given frequencies of ground motion to profile depth. V_S^{QWL} is recursively related to depth as a function of frequency – lower frequencies average over greater depths (z):

$$V_S^{\text{QWL}}(f) = f\lambda = 4fz \quad (5)$$

In fact, V_{S30} is a discrete sample of the quarter wavelength–frequency–depth distribution for a site (Poggi *et al.* 2011). The advantage of using the quarter-wavelength average velocity is its frequency dependence: we add a significant degree of information regarding the amplification potential of a site. For example, Joyner *et al.* (1981) used V_S^{QWL} to estimate site amplification, while Edwards *et al.* (2011) and Poggi *et al.* (2012) showed how the horizontal-to-vertical ratio of ground motion at a site can be modelled as a function of V_S^{QWL} .

V_S^{QWL} also allows us to investigate hard-rock sites to a greater potential. There are 32 recording sites (less than 5 per cent) with $V_{S30} > 1000 \text{ m s}^{-1}$ and only 10 with $V_{S30} > 1200 \text{ m s}^{-1}$ in the KiK-Net database used, making exhaustive analysis difficult. However, we can nevertheless look at specific frequencies, where we know that the corresponding V_S^{QWL} at a given site is greater than, for example, 1000 m s^{-1} . This is because lower frequency motions are insensitive to shallow low velocity layers: therefore the effective velocity profile ‘sampled’ by a $T = 2 \text{ s}$ wave, is different to that

of a $T = 0.1 \text{ s}$ wave. We can therefore add a significant number of sites (albeit within a restricted frequency band) to the analysis where, for instance, V_{S30} is decreased due to a thin upper low-velocity layer of a few metres. In such cases, whilst amplification is expected, it is only at high frequency: the V_S^{QWL} highlights this by assigning appropriately high average velocities (corresponding to deep penetration depths) to low frequency ground motion. Clearly, this is most applicable to longer periods, such as 0.5–2 s, where the sampling depths for V_S^{QWL} extend to the order 100 m.

In this analysis, we use only the original response spectra (uncorrected for site effects). The GMPE prediction is made according to the corresponding site's class or V_{S30} value. First, residual misfit against magnitude, distance, V_{S30} and V_S^{QWL} was calculated for two GMPEs using site-class as input: Zhao *et al.* (2006) (at distances to 300 km) and Akkar & Bommer (2010) (at distances to 100 km). Naturally the Japanese model of Zhao *et al.* (2006) performed better overall when looking at the magnitude and distance residuals. However, both models show systematic residual trends with distance and magnitude (as already observed for ZETAL06 in Fig. 4). Since we are interested in the performance of the GMPEs relative to the site component of prediction, we therefore make an initial adjustment of the GMPEs by modifying the coefficients related to (i) overall spectral amplitude, (ii) distance dependence. This is achieved by fitting the following functional term to the misfit, where Y_R/Y_{GMPE} is the ratio of the corrected prediction (Y_R) and original GMPE prediction (Y_{GMPE}) (Fig. 8)

$$Y_R/Y_{\text{GMPE}} = b_0 = a_0 + a_1 R_{\text{epi}} \quad (6)$$

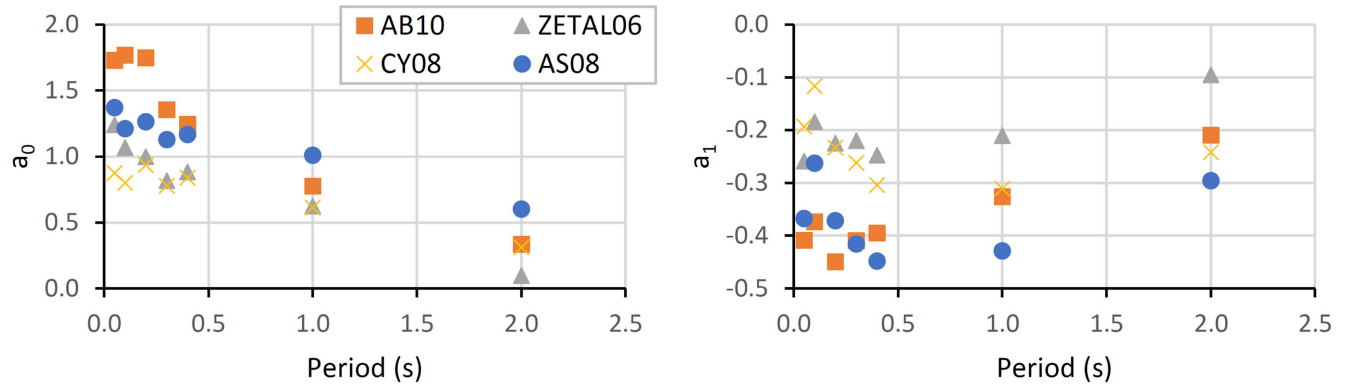


Figure 8. Adjustment to GMPE coefficients a_0 and a_1 (eq. 6) to account for stronger observed attenuation.

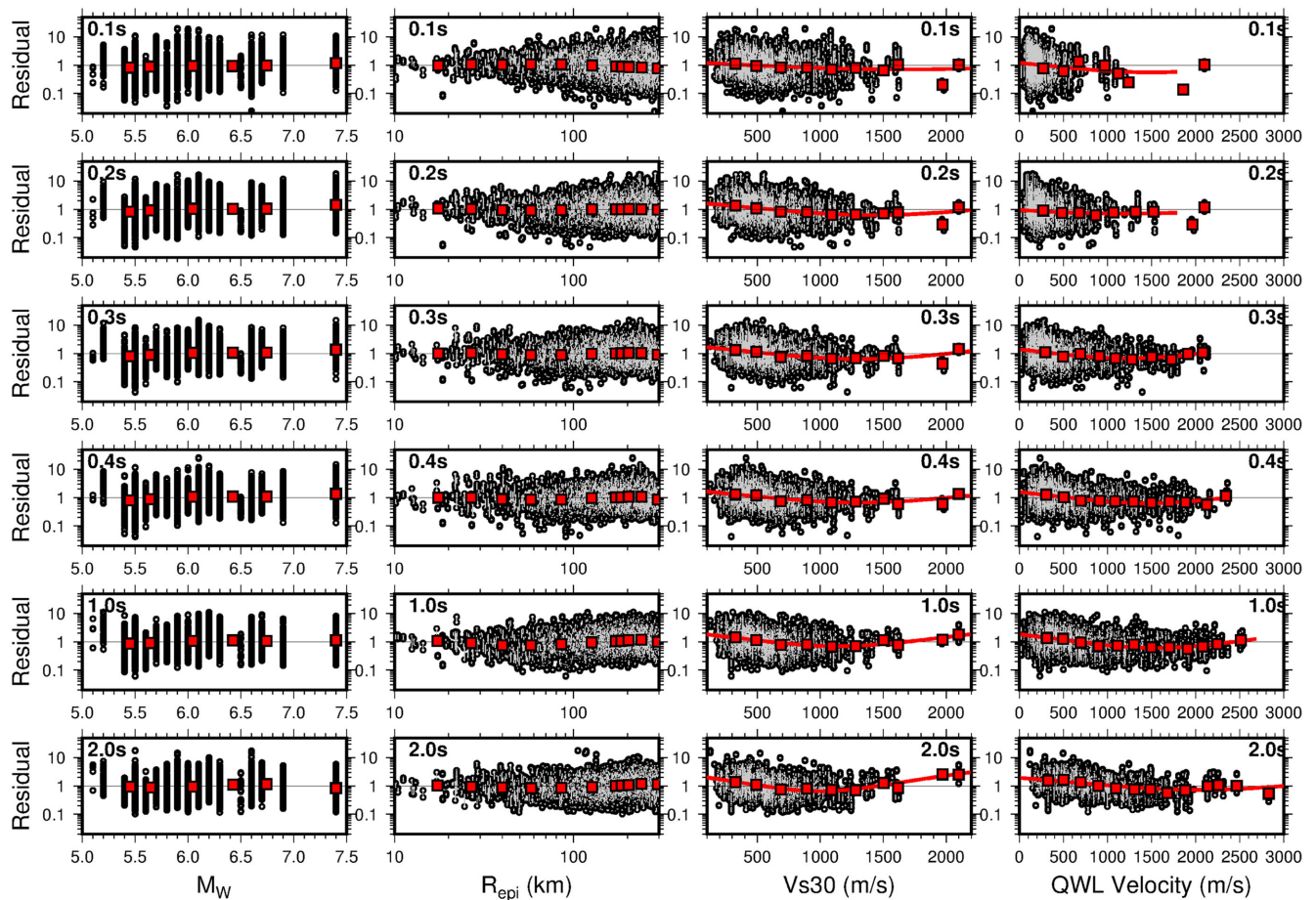


Figure 9. Residual misfit of the Zhao *et al.* (2006) plotted against M , distance, V_{S30} and V_S^{QWL} . Squares indicate the mean residual misfit. Where present, the thick lines indicate the best-fitting quadratic fit to the residual trend.

Whether with or without the distance correction, a trend in the residuals of both ZETAL06 and AB10 versus V_S^{QWL} is apparent (Figs 9 and 10, respectively): ground motions corresponding to low V_S^{QWL} tend to be underpredicted, whilst those corresponding to high V_S^{QWL} are systematically overpredicted. V_S^{QWL} consistent with those of the reference profile used in the previous analyses ($V_{S30} = 1350 \text{ m s}^{-1}$, Figs 6b and 7b) are approximately 1400 m s^{-1} to 2600 m s^{-1} in the range 10 to 1 Hz respectively. For both V_{S30} and V_S^{QWL} the GMPEs tend to consistently overpredict the data in this range. This suggests that the site-class based GMPEs of

Zhao *et al.* (2006) and Akkar & Bommer (2010) will overpredict ground motion at hard-rock sites. We note that for both models, the trend with V_{S30} disappears for short periods (0.1 s and lower), which correspond to quarter-wavelength depths of the upper tens of metres: typical depths over which to base geotechnical site classification.

We next tested three further models (two used in the PEGASOS Refinement Project) that used V_{S30} directly as a predictor variable: Chiou & Youngs (2008) (CY08; distances to 200 km; Fig. 11), Abrahamson & Silva (2008) (AS08; distances to 200 km; Fig. 12) and the NGA-West2 model of Boore *et al.* (2014) (BSSA14;

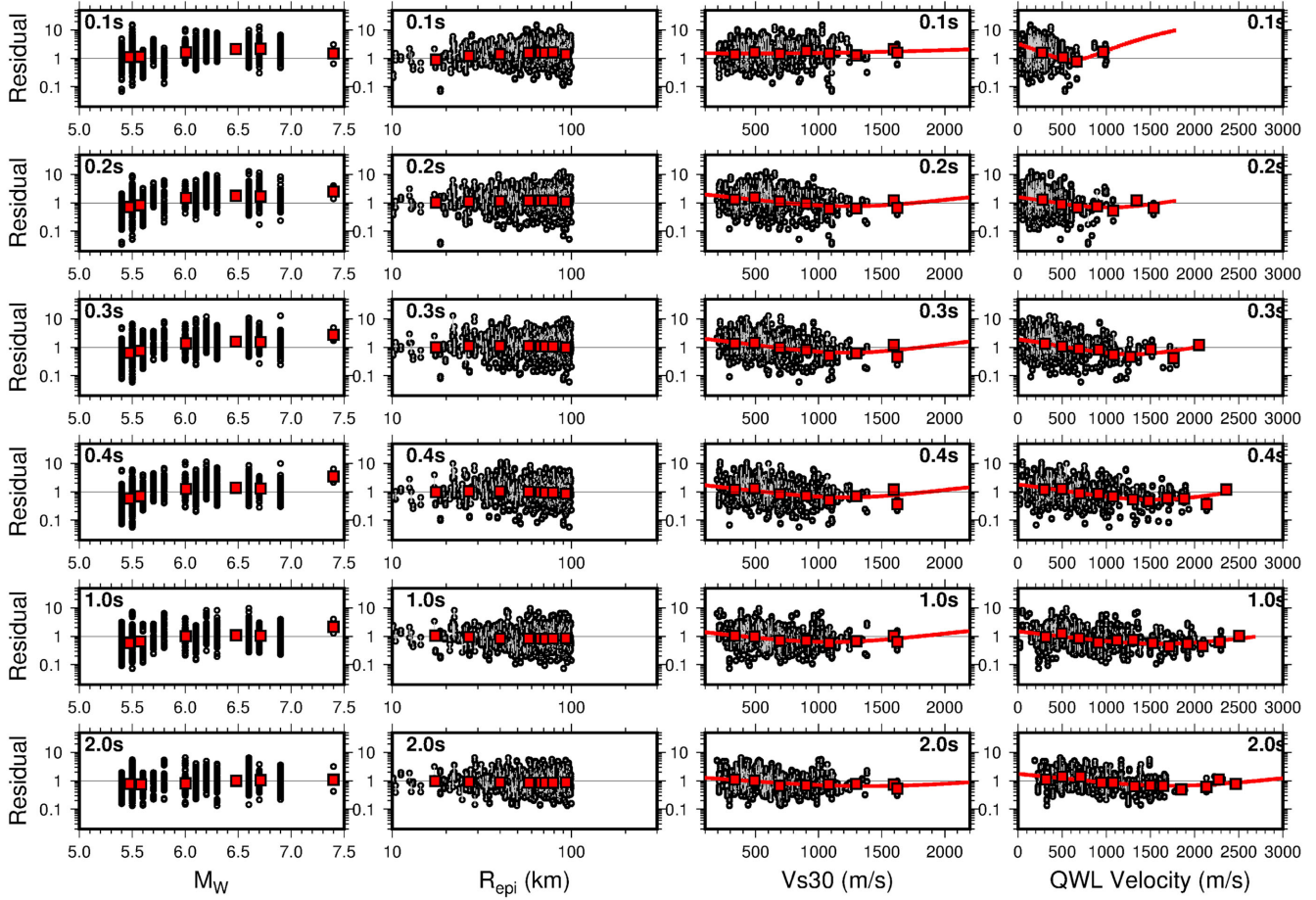


Figure 10. Residual misfit of the Akkar & Bommer (2010) plotted against M , distance, V_{s30} and V_s^{QWL} . Squares indicate the mean residual misfit. Where present, the thick lines indicate the best-fitting quadratic fit to the residual trend.

distances to 300 km; Fig. 13). Due to the incorrect attenuation (for Japan) in CY08 and AS08, we again initially noted a systematic offset of the residuals with data set average overprediction typical at all frequencies, in addition to a distance trend. Since the models were not developed using a significant amount of Japanese data this is not surprising and highlights the effect of regional variation in attenuation. Indeed, in the NGA-West2 GMPEs, such as the model of Boore *et al.* (2014) used here, a term is now included to account for this high rate of decay. All GMPEs apart from BSSA14 are therefore again corrected for a simple distance dependency (eq. 6, Fig. 8) before calculating the residuals shown in Figs 11 and 12. BSSA14 was used with the Japan-specific predictions enabled. We note that the residual misfit trend with V_{s30} is somewhat reduced for these models. For V_s^{QWL} , however, a trend remains for moderate periods (1–0.3 s). As for the site class models, for short periods (0.1 s and less), corresponding to quarter-wavelength depths of tens of metres, we observe negligible trends with V_{s30} or V_s^{QWL} .

A summary of the trends in residual misfit versus quarter-wavelength velocity are given in Fig. 14. It is clear that the form of the misfit is consistent between each GMPE (despite their difference functional forms), therefore an average adjustment factor is proposed such that (Table 1):

$$Y_{\text{site}}/Y_{\text{GMPE}} = b_0 + b_1 V_s^{QWL} + b_2 (V_s^{QWL})^2 \quad (7)$$

where $Y_{\text{site}}/Y_{\text{GMPE}}$ is the ratio of the site corrected prediction (Y_{site}) and original GMPE prediction (Y_{GMPE}). Y are values of

PSA. This adjustment, which adds a dependency of V_s^{QWL} , in addition to V_{s30} can be used to tailor site-specific GMPE predictions, when the full V_s profile is known. The correction appears to be mostly period independent, such that a single correction can be applied across the period range (2–0.3 s). At shorter periods (0.1 s) we observed that there was limited residual trend: therefore the correction should not be applied here and may transition between periods of 0.3 s (eq. 7) and 0.1 s (no correction).

4.4 Stochastic simulations

Analysis of ground-motion residuals using GMPEs developed for both Japan and elsewhere have indicated that for subselections of rock and hard-rock sites (or high V_s^{QWL}), the selected GMPEs tend to overpredict ground motion. In order to account for site-specific amplification effects in ground-motion prediction across broad range of periods relevant to engineering, stochastic simulation is a popular choice (Campbell 2003). For each recording in our database, we therefore simulated the expected 5 per cent damped PSA spectrum using the code SMSIM (Boore 2003). The input model for the simulation was based on the model of Edwards & Fäh (2013), which was developed during the PRP using Swiss instrumental data and calibrated with macroseismic data in the high-magnitude range. The model consists of a Brune (1970) earthquake spectral source model, shaking duration model, a

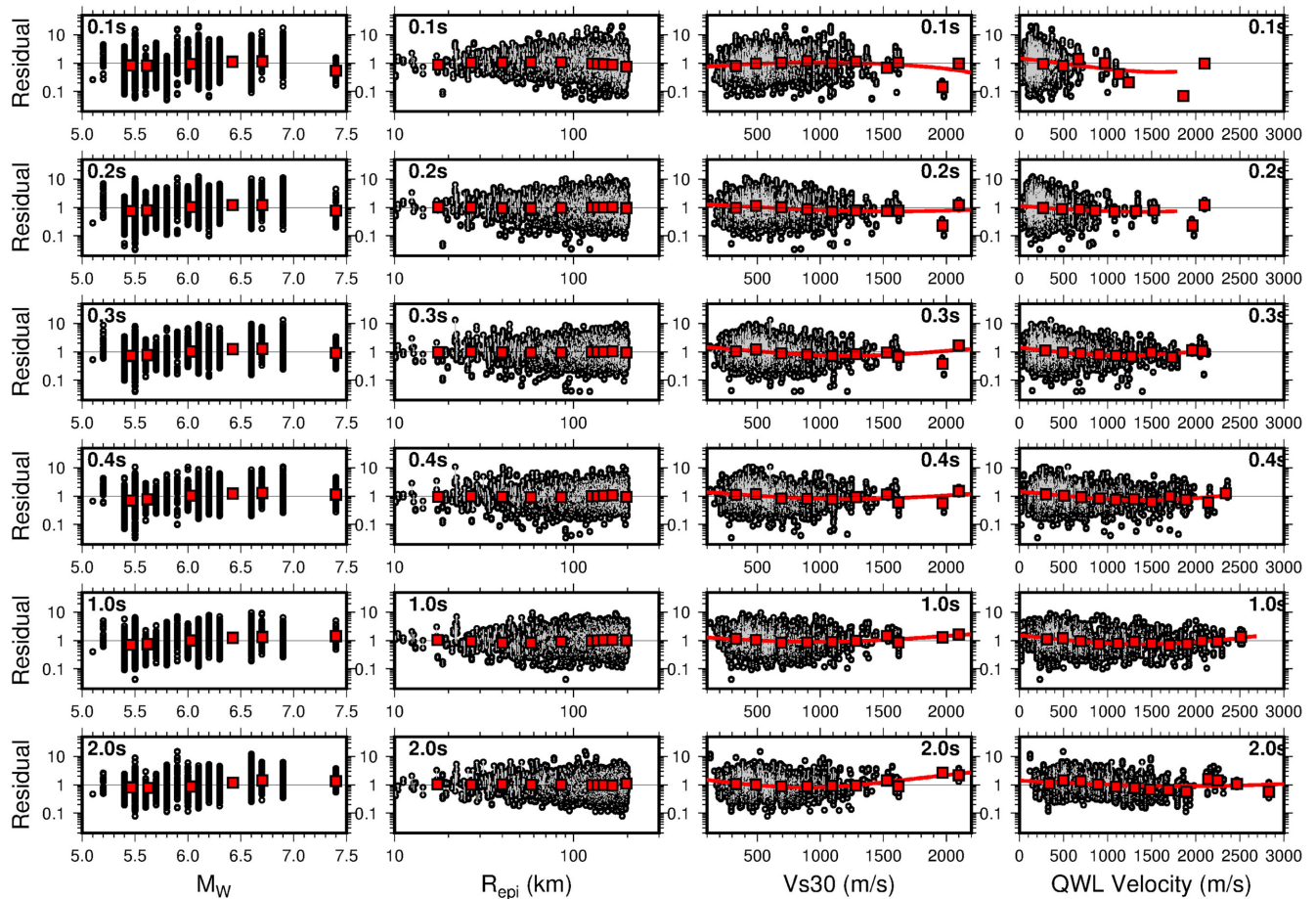


Figure 11. Residual misfit of the Chiou & Youngs (2008) plotted against M , distance, V_{s30} and V_{s}^{QWL} . Squares indicate the mean residual misfit. Where present, the thick lines indicate the best-fitting quadratic fit to the residual trend.

description of path attenuation, and site specific attenuation for the Swiss reference rock V_s profile and corresponding elastic SH amplification determined by Poggi *et al.* (2011). In order to include finite fault geometric effects, the model implements the pseudo-finite fault distance metric R_{EFF} (Boore 2009). This takes input R_{JB} (closest distance to the surface projection of the fault) along with fault dimensions, orientation and hypocentral depth (H) in order to provide a metric which appropriately scales the near-source ground motion based on random hypocentre location and equal energy radiation over the fault.

We made a basic adjustment in the stochastic model for:

- (i) the reference V_s profile, by implementing the corresponding amplification for a hard-rock Japanese reference velocity model (Poggi *et al.* 2013), as used as the target for the previous empirical analyses;
- (ii) the crustal geometrical attenuation model $1/R^{1.29}$ consistent with frequency independent Q (Poggi *et al.* 2013);
- (iii) the stress-parameter: 3, 6, 9 and 12 MPa.

The input site terms were taken from either (a) empirical average anelastic Fourier amplification (Fig. 15), or (ii) from 1-D SH anelastic amplification (Fig. 16). A 9 MPa model was found to lead to the best fit, which is higher than that used in Switzerland (6.3 MPa), but close to the value of around 10 MPa found for European and Middle East earthquakes (Edwards & Fäh 2013). When using the empirical amplification input the model shows an

overprediction at low frequency (e.g. 1 Hz) and $M < 6.25$ but the distance trend in the residuals is less significant than when using ZETAL06. When using the 1-D SH amplification input the model predicts the ground motions well across the range of analysed frequencies, although tends to underpredict for $M > 6.5$. At distances greater than 100 km, the model shows evidence of not accounting for a frequency dependent attenuation, with too strong attenuation at long-period, and too weak attenuation at short periods. We note that since this is not a regionally derived model, but rather a Swiss-based model adjusted to Japanese ground motions, we do not focus on the detailed behaviour of the residuals. For example, a three-segment geometrical decay model and frequency-dependent Q model should reduce the misfit further, particularly at very near and far distances.

While the stochastic simulation model is not a native model, having been adapted from the Swiss model with only basic modifications, we can regardless see the impact of including site-specific information relative to the GMPE of ZETAL06. Using the same data (distances less than 200 km) we compared the observed misfit in the predictions using the GMPE of Zhao *et al.* (2006) and the simulation approach. The uncertainty was defined by:

$$\sigma^2 = \frac{1}{N} \sum_{n=1}^N (Y_n - \ln(f_n(\mathbf{X}_{es}, \Theta)))^2, \quad (8)$$

where Y_n is the natural log of the observed ground motion and $f_n(\mathbf{X}_{es}, \Theta)$ is that predicted by the model for observation n . \mathbf{X}_{es} is

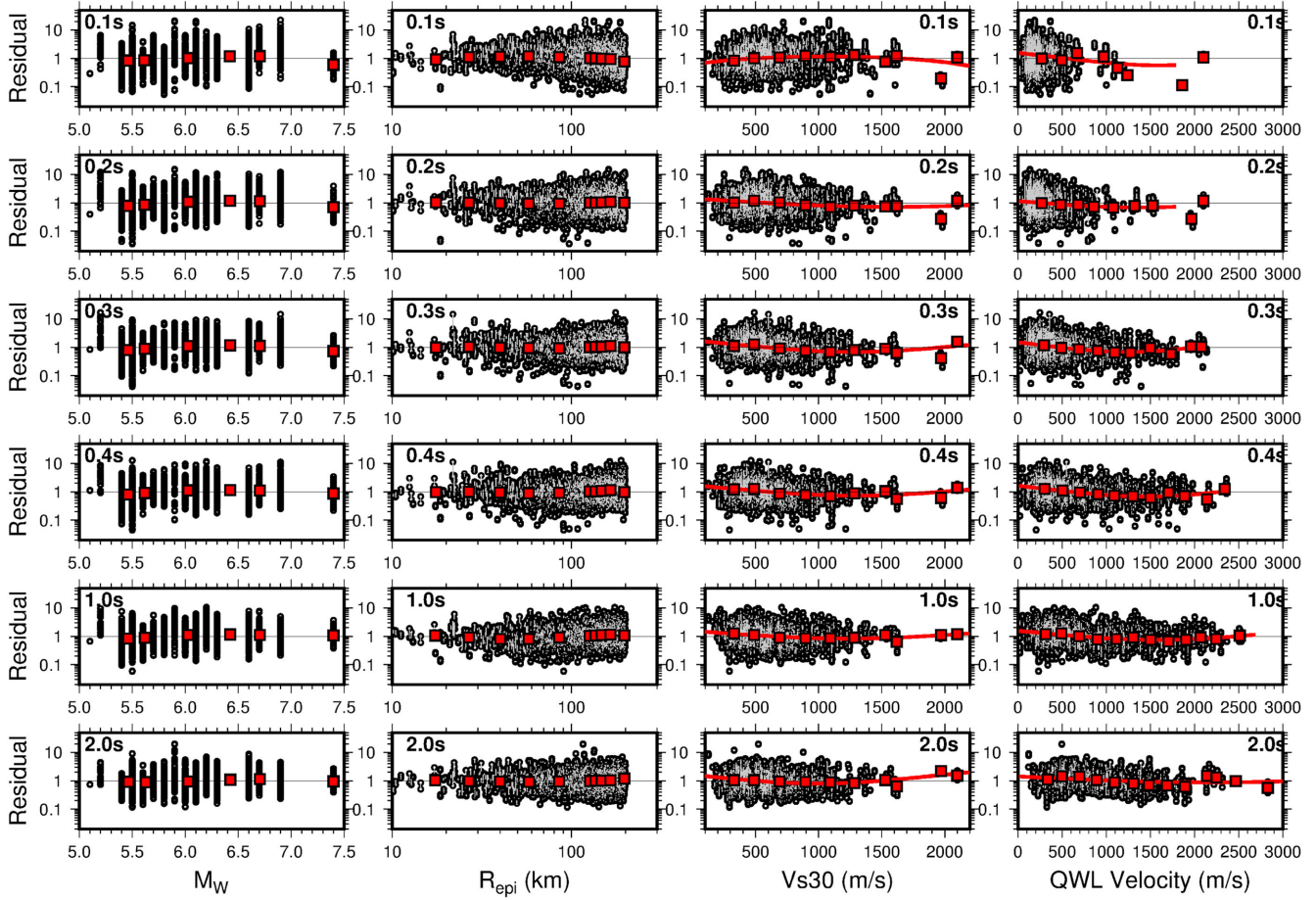


Figure 12. Residual misfit of the Abrahamson & Silva (2008) plotted against M , distance, V_{S30} and V_S^{QWL} . Squares indicate the mean residual misfit. Where present, the thick lines indicate the best-fitting quadratic fit to the residual trend.

the vector of independent parameters (magnitude, distance. . .) and Θ is the vector of model parameters. The total sigma can be split into between- and within-event terms, τ and ϕ respectively. If they are uncorrelated, then:

$$\sigma = \sqrt{\tau^2 + \phi^2} \quad (9)$$

with ϕ given by

$$\phi = \sqrt{\phi_{S2S}^2 + \phi_{SS}^2}, \quad (10)$$

ϕ_{SS} represents the single-site within-event variability, while ϕ_{S2S} is the site to site variability (Fig. 17).

4.5 Hard-rock ground motion: simulation

The previous analysis showed that the simulation based approach provided significantly reduced within-event component over the complete data set. This was possible due to being able to use all available information known about the sites (i.e. site specific amplification and attenuation). We finally take the same rock and hard-rock site data set (corrected to the bedrock using the empirical anelastic amplification) with $V_{S30} > 800 \text{ m s}^{-1}$ (as Fig. 6 for ZETAL06) and compare the RVT simulation predictions in terms of the intra-event residuals (calculated over the whole data set) with those from ZETAL06 (Fig. 18).

The performance of both the RVT simulation model and ZETAL06 for this hard-rock data set is similar, with median predictions

falling within the one-sigma range of the data distribution. There is systematic overprediction of low frequency (1.0 Hz) data, which reduces at 3.0 Hz. The performance is similar across the range of periods. The fact that the intra-event variability for the rock sites is similar for both RVT simulation and GMPEs indicates that the benefit of including site-specific amplification comes when looking at soil sites. However, the simulations have the advantage of a clearly defined rock reference on which to base any further adjustment.

5 DISCUSSION AND CONCLUSIONS

Empirical based GMPEs are a useful tool for describing and predicting ground motion for typical scenarios. However, in current seismic hazard analyses, state-of-the-art approaches aim to decouple bedrock and near-surface ground-motion prediction. The prediction of bedrock level ground motion presents a significant challenge for empirical approaches, where limited recordings at hard rock mean that models are at best not robust, and may show significant misfit bias. One solution to fill this data-gap is the introduction of simulation data into GMPEs, or even totally simulation based approaches.

Epistemic uncertainty is accounted for in seismic hazard analyses through the logic-tree approach (McGuire 2008). Several GMPEs are typically tested and applied (e.g. Delavaud *et al.* 2012b), with each using different predictor variables, model form or background data sets. Hazard is then computed based on subsequent weighting

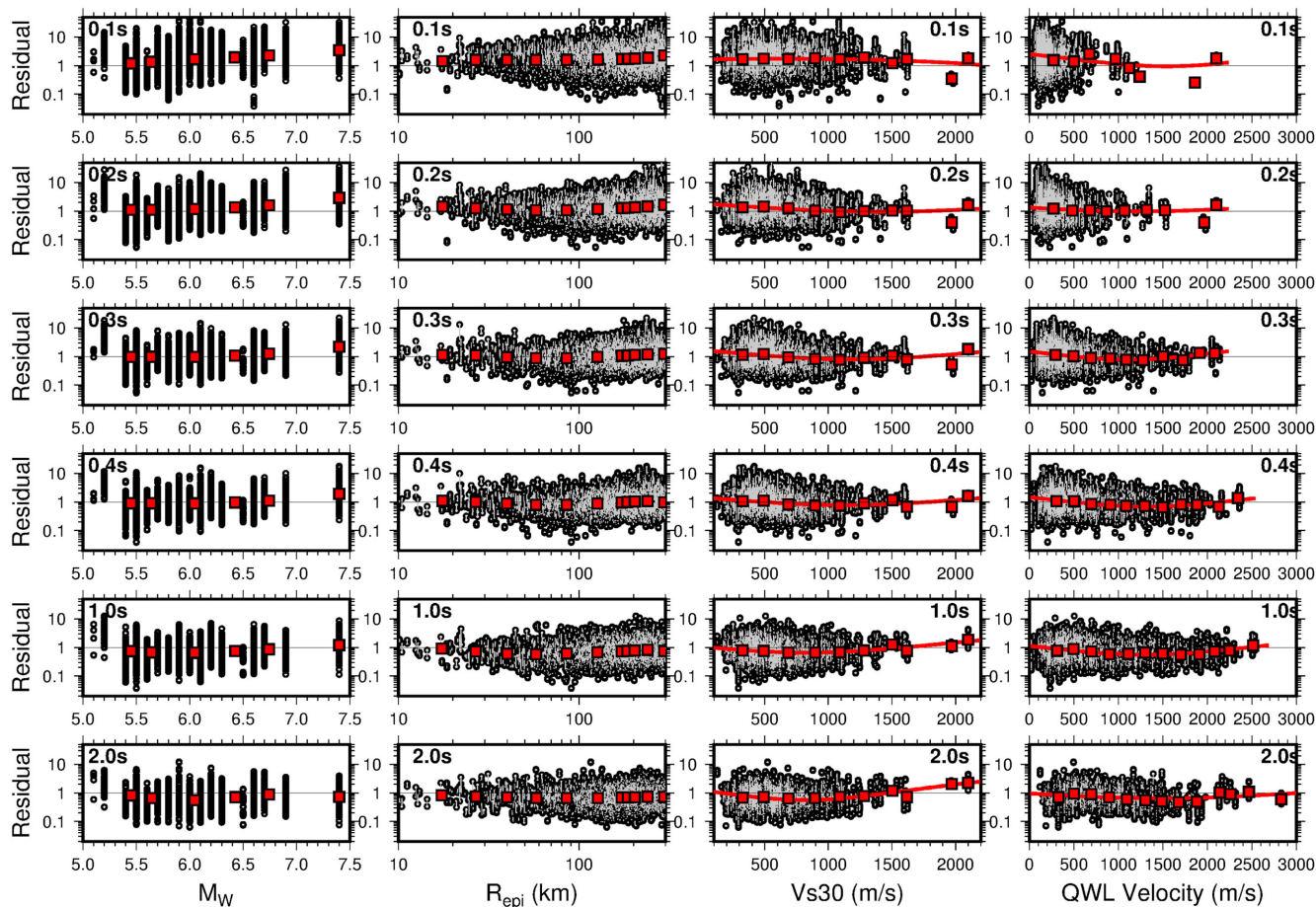


Figure 13. Residual misfit of the Boore *et al.* (2014) GMPE plotted against M_w , distance, V_{s30} and V_s^{QWL} . Squares indicate the mean residual misfit. Where present, the thick lines indicate the best-fitting quadratic fit to the residual trend.

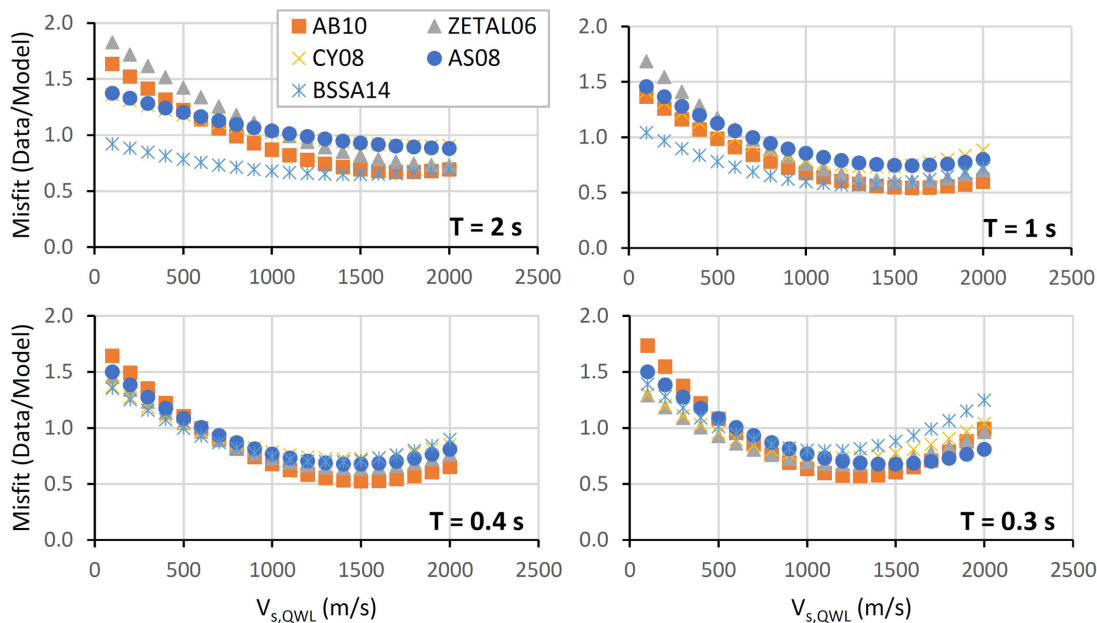


Figure 14. Average residual misfit based on fitting quadratic form to the residuals against V_s^{QWL} in Figs 9–13.

Table 1. Average coefficients determined for eq. (7).

Period (s)	b_0	b_1	b_2
2	1.4994E+00	-7.7797E-04	2.0915E-07
1	1.5043E+00	-1.1538E-03	3.8598E-07
0.4	1.5903E+00	-1.3007E-03	4.5142E-07
0.3	1.5786E+00	-1.4130E-03	5.6439E-07
Average	1.5431E+00	-1.1614E-03	4.0274E-07
Standard deviation	0.0479905	0.00027677	1.486E-07

of branches of the logic tree, which should reflect an expert's (or an expert panel's) degree of belief and appropriately cover the epistemic uncertainty. However, while such approaches are considered best-practice (Bommer & Scherbaum 2008), it remains difficult to assess if the entire range of epistemic uncertainty is appropriate. While empirical GMPEs provide a user-friendly tool for seismic hazard analysis, the difficulty to associate them to physical processes means that epistemic uncertainty and host-target adjustments are difficult to quantify. In particular, V_{S30} as a reference is inadequate because it is not directly related to frequency dependent wave propagation, and does not account for characteristic velocity profiles in a particular region.

We initially assessed the performance of a Japanese GMPE (ZETAL06) by comparing its predictions to our data set. The GMPE was based on data from strong-motion networks K-Net and KiK-Net. Systematic deviations in residual misfit behaviour were observed. An explanation for the possible different amplification be-

haviour at K-Net (included in ZETAL06) and KiK-Net (in both ZETAL06 and used here) sites is possible if we consider the situation of the different networks. The KiK-Net sites are free-field surface accelerometers co-located with borehole instrumentation (an accelerometer and high-sensitivity short-period seismometer). The location of KiK-Net sites is typically where the bedrock is relatively shallow (often within 100–200 m)—such that the co-located borehole instrumentation reaches the bedrock. KiK-Net sites therefore represent a subset of the possible site types in Japan. They are not (on average) representative of deep sedimentary basins, which tend to induce amplification and resonance at low frequencies (e.g. 0.5–1 Hz)—and which are instrumented by K-Net. This may partially explain the misfit between the KiK-Net data and ZETAL06 predictions at low frequency (Fig. 4). The differences shown here highlight the fact that GMPEs are simplifications of complex phenomena. In terms of V_{S30} , a variety of site responses are possible, with the GMPE ideally predicting the average response at a given V_{S30} , or within a range of V_{S30} (site-class). If the response of subset of sites within a given site class or V_{S30} range is systematically different to the average used during the model's derivation then the GMPE's average site response will not necessarily be unbiased.

In order to extend the analysis of hard-rock sites, we used the quarter-wavelength velocity domain. By exploiting the frequency-depth sensitivity of the wave-field, we can add many long-period observations (sensitive to deeper and typically rather high average velocities). The analysis showed that trends with V_S^{QWL} in the residual misfit of five GMPEs were present, both for class-based models: Zhao *et al.* (2006) and Akkar & Bommer (2010); and

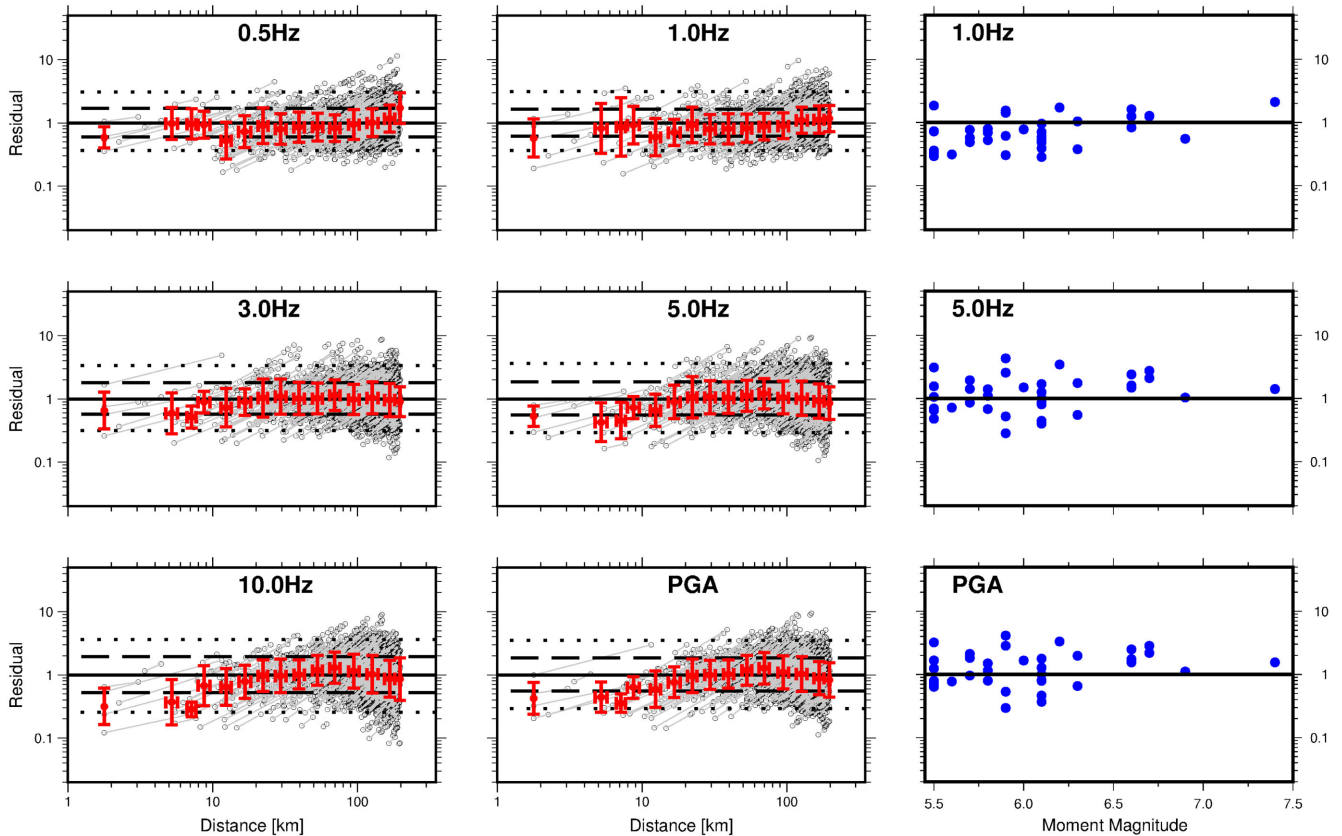


Figure 15. Residual misfit (data/model) of the Japanese reference rock stochastic model versus distance (left, intra-event) and magnitude (right, inter-event). The model is for a strike-slip event, with site-specific anelastic empirical amplification used relative to the $V_{S30} = 1350 \text{ m s}^{-1}$ reference rock model of Poggi *et al.* (2013). Lines join the R_{rup}^{lower} and R_{rup}^{upper} model estimates for a single recording.

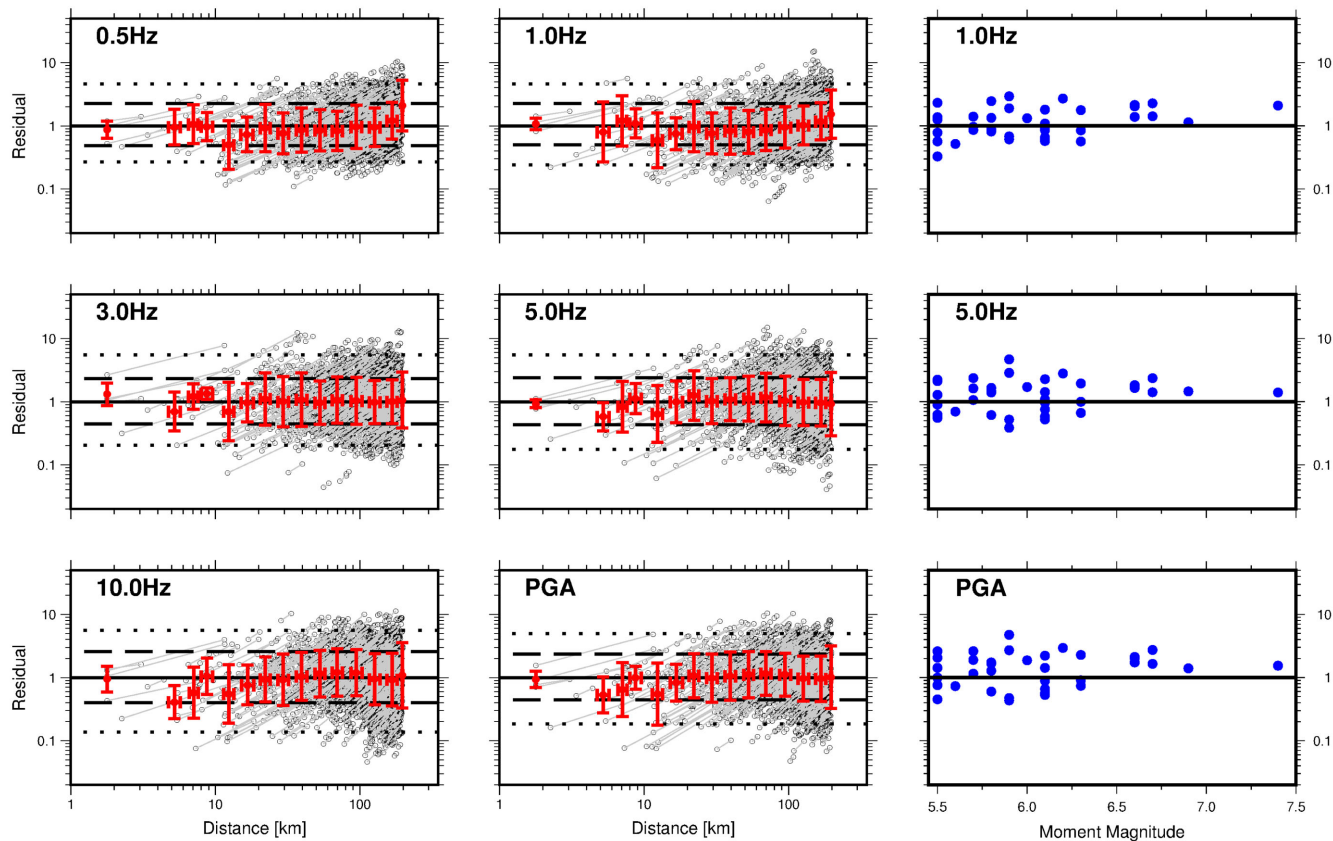


Figure 16. Residual misfit versus distance and magnitude for sites corrected to the bedrock using site-specific 1-D anelastic SH amplification. Predictions are made using the adjusted RVT model of Edwards & Fäh (2013).

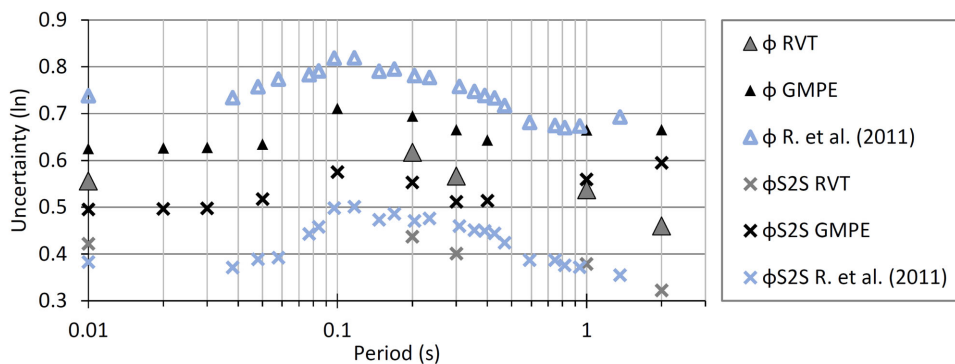


Figure 17. Comparison of prediction uncertainty (natural log) between the empirical (GMPE) and simulation (RVT) models. The uncertainty from Rodriguez-Marek *et al.* (2011) is shown for comparison. As shown in the figure, the simulation based predictions typically result in lower within-event uncertainty than the empirical based predictions over all sites (i.e. not only limited to hard-rock sites).

V_{S30} based GMPEs: Abrahamson & Silva (2008), Chiou & Youngs (2008) and Boore *et al.* (2014). The analysis showed that the misfit bias had minima in the quadratic trend in the range of quarter-wavelength average velocity $1000\text{--}2000\text{ m s}^{-1}$, particularly at the periods which are more sensitive to variations in the upper 100 m or so (e.g. 0.3 s). All GMPEs therefore overestimated the ground motion at high V_{S30}^{QWL} (Fig. 14). At short periods, consistent with quarter-wavelength depths over which sites are classified (i.e. upper tens of metres), the models performed without misfit trends in V_{S30} or V_{S30}^{QWL} .

Finally, we implemented a simulation based model, adapted from a Swiss pseudo finite-fault stochastic model (Edwards & Fäh 2013). The changes to the simulation model were (a) the reference rock,

which was the $V_{S30} = 1350\text{ m s}^{-1}$ profile of (Poggi *et al.* 2013) and the corresponding near-surface attenuation; and (b) the regional attenuation model (Poggi *et al.* 2013). Site-specific amplification and attenuation for the Japanese KiK-Net sites was also implemented. In the case of using theoretical 1-D SH based amplification, a better fit was found in particular at closer distances smaller than 10 km. The stress parameter was increased from 6.3 to 9 MPa.

Using the RVT simulation model, we found that the average performance was consistent with the empirical model over all sites. For the largest events, with $M > 6.5$, the RVT model tended to under-predict motions, suggesting that a higher stress-parameter model (or increasing with M) should be adopted. This highlights the need for appropriate epistemic uncertainty in the stress-parameter to be

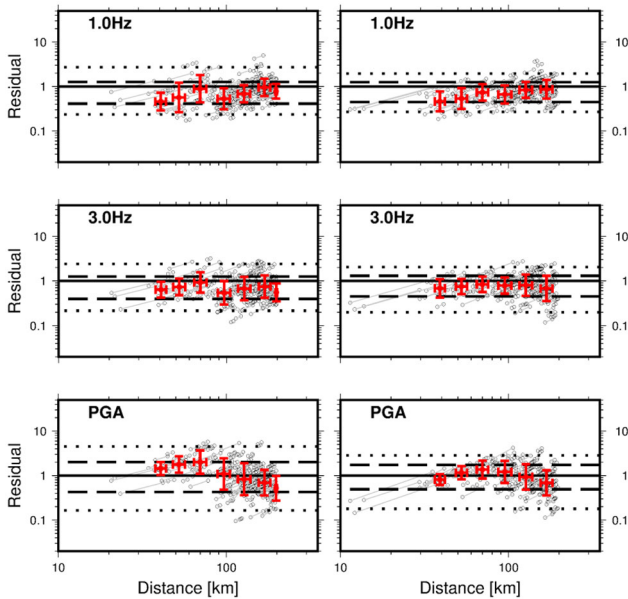


Figure 18. Intra-event misfit of the rock ($V_{S30} > 800 \text{ m s}^{-1}$) data compared to the (left) the GMPE of ZETAL06 and (right) RVT simulations using the empirical amplification functions.

included in simulation models (even when relatively large earthquakes are available in the calibration database). Residual analysis for sigma showed that the within-event term, associated mainly to the site-to-site variability and within-site variability, was significantly reduced due to the simulation model utilising site-specific as opposed to a proxy-based amplification. The performance of the simulation model for the subselection of rock and hard-rock sites was comparable to the empirical approach. Evidence of frequency-dependent attenuation nevertheless shows the limitation of simplified simulation approaches. Further work should be undertaken to improve stochastic based simulation models, particularly in terms of inter-event variability, however, the analysis shown here shows that in their current form they provide predictions that are consistent with empirical approaches, particularly for scenarios where limited data are available, and are easier to adjust. Finally, future empirical based approaches should pay attention to estimating epistemic uncertainty such that their limitations can be appreciated. For future applications of ground-motion models in PSHA, it is clear that region- or even path-specific wave propagation must be accounted for in order to reduce the epistemic uncertainty related to within-event variability.

The context of this study was to assess the GMPEs used in the PRP. The conclusions are therefore linked to the models used therein and also to the Japanese data used for comparison. The model applicability has been extended by analysing a more recent NGA-2 model, which showed similar behaviour and overestimation of rock—to hard-rock predictions. It may be argued that the results presented here are applicable only to Japanese data. More recent GMPEs (Boore *et al.* 2014; Chiou & Youngs 2014) do include a Japan-specific predictor. However, this is only related to the decay with distance and therefore does not affect our interpretation (where corrections for this attenuation effect were explicitly considered). We believe the dependence of ground-motion misfit with V_S^{QWL} is related to the oversimplified use of V_{S30} for predicting site amplification in GMPEs. Boore *et al.* (2011) showed that the dependence of V_S on depth could be reasonably extrapolated from knowledge

of shallow velocities in both California and Japan—which would suggest that V_{S30} is a suitable proxy for V_{Sx} assuming a gradient model. However, deriving a GMPE based on V_{S30} risks smoothing the spectral shape of amplification at lower velocity sites into regions where data are sparse. We therefore argue for a more physically robust approach for amplification determination—which can simply be achieved through the use of V_S^{QWL} in GMPEs. Alternatively, empirical corrections for V_{S30} based models (as derived here) can be developed to account for these effects.

Importantly, this study has shown that recent and current GMPEs (even those with region-specific parameters) do not universally predict unbiased earthquake ground motion for sites in the rock to hard-rock categories. Current practice in state-of-the-art projects mitigates this effect by using GMPEs only at V_{S30} values where they are considered robust, then making physically based adjustments to correct them to a rock reference. However, this is not ideal and introduces significant epistemic uncertainty. The overestimation of ground-motion amplitudes may simply be due to artefacts of low- V_S amplification effects in the data-poor model space at high V_S . Regardless of the reason for the overestimation, it is clear that the way forward must involve the implementation of site-specific capabilities in GMPEs—for instance through the use of V_S^{QWL} and the quarter-wavelength impedance contrast (Poggi *et al.* 2012). A wealth of information is available in terms of seismological source-path and site effects (on which stochastic or RVT models are based) which clearly has the possibility to reduce uncertainties in GMPEs (Baltay *et al.* 2017)—the focus in future years should be to integrate complementary fields of research to provide robust hybrid simulation-empirical models that make full use of the available knowledge.

ACKNOWLEDGEMENTS

This project was funded by the Swiss Federal Nuclear Safety Inspectorate (ENSI). We thank the NIED for making the waveform data available. We thank the associate editor and two anonymous reviewers for their useful comments, which have helped improve this paper.

REFERENCES

- Abrahamson, N. & Silva, W., 2008. Summary of the Abrahamson & Silva NGA ground-motion relations, *Earthq. Spectra*, **24**, 67–97.
- Abrahamson, N. *et al.*, 2008. Comparisons of the NGA ground-motion relations, *Earthq. Spectra*, **24**, 45–66.
- Akkar, S. & Bommer, J.J., 2006. Influence of long-period filter cut-off on elastic spectral displacements, *Earthq. Eng. Struct. Dyn.*, **35**, 1145–1165.
- Akkar, S. & Bommer, J.J., 2010. Empirical equations for the prediction of PGA, PGV, and spectral accelerations in Europe, the Mediterranean region, and the Middle East, *Seismol. Res. Lett.*, **81**, 195–206.
- Akkar, S. *et al.*, 2014. Reference database for seismic ground-motion in Europe (Resorce), *Bull. Earthq. Eng.*, **12**, 311–339.
- Al Atik, L., Kottke, A., Abrahamson, N. & Hollenback, J., 2014. Kappa (Kappa) scaling of ground-motion prediction equations using an inverse random vibration theory approach, *Bull. seism. Soc. Am.*, **104**, 336–346.
- Ancheta, T.D. *et al.*, 2014. NGA-WEST 2 database, *Earthq. Spectra*, **30**, 989–1005.
- Aoi, S., Kunugi, T. & Fujiwara, H., 2004. Strong-Motion seismograph network operated by NIED: K-Net and Kik-Net, *J. Japan Assoc. Earthq. Eng.*, **4**, 65–74.
- Atkinson, G.M. & Boore, D.M., 2006. Earthquake ground-motion prediction equations for Eastern North America, *Bull. seism. Soc. Am.*, **96**, 2181–2205.

- Baltay, A.S., Hanks, T.C. & Abrahamson, N.A., 2017. Uncertainty, variability, and earthquake physics in Ground-Motion prediction Equations, *Bull. seism. Soc. Am.*, in press, doi: 10.1785/0120160164.
- Bindi, D., Pacor, F., Luzi, L., Puglia, R., Massa, M., Ameri, G. & Paolucci, R., 2011. Ground motion prediction equations derived from the Italian strong motion database, *Bull. Earthq. Eng.*, **9**, 1899–1920.
- Bommer, J.J. & Scherbaum, F., 2008. The use and misuse of logic trees in probabilistic seismic hazard analysis, *Earthq. Spectra*, **24**, 997–1009.
- Bommer, J.J., Dost, B., Edwards, B., Stafford, P.J., van Elk, J., Doornhof, D. & Ntinalexis, M., 2016. Developing an application-specific ground-motion model for induced seismicity, *Bull. seism. Soc. Am.*, **106**, 158–173.
- Bommer, J.J. *et al.*, 2017. Framework for a ground-motion model for induced seismic hazard and risk analysis in the groningen gas field, the Netherlands, *Earthq. Spectra*, **33**, 481–498.
- Boore, D.M., 2003. Simulation of ground motion using the stochastic method, *Pure appl. Geophys.*, **160**, 635–676.
- Boore, D.M., 2005. On pads and filters: processing strong-motion data, *Bull. seism. Soc. Am.*, **95**, 745–750.
- Boore, D.M., 2009. Comparing stochastic point-source and finite-source ground-motion simulations: smsim and exsim, *Bull. seism. Soc. Am.*, **99**, 3202–3216.
- Boore, D.M. & Joyner, W.B., 1997. Site amplifications for generic rock sites, *Bull. seism. Soc. Am.*, **87**, 327–341.
- Boore, D.M., Thompson, E.M. & Cadet, H., 2011. Regional correlations of V_{S30} and velocities averaged over depths less than and greater than 30 meters, *Bull. seism. Soc. Am.*, **101**, 3046–3059.
- Boore, D.M., Stewart, J.P., Seyhan, E. & Atkinson, G.M., 2014. Nga-West2 equations for predicting Pga, Pgv, and 5% damped psa for shallow crustal earthquakes, *Earthq. Spectra*, **30**, 1057–1085.
- Bora, S., Scherbaum, F., Kuehn, N. & Stafford, P., 2013. Fourier spectral- and duration models for the generation of response spectra adjustable to different source-, propagation-, and site conditions, *Bull. Earthq. Eng.*, **1–27**, doi: 10.1007/s10518-013-9482-z.
- Bora, S.S., Scherbaum, F., Kuehn, N. & Stafford, P., 2016. On the relationship between fourier and response spectra: implications for the adjustment of empirical ground-motion prediction equations (Gmpes), *Bull. seism. Soc. Am.*, **106**.
- Brune, J.N., 1970. Tectonic stress and spectra of seismic shear waves from earthquakes, *J. geophys. Res.*, **75**, 4997–5009.
- Campbell, K.W., 2003. Prediction of strong ground motion using the hybrid empirical method and its use in the development of ground-motion (Attenuation) relations in eastern North America, *Bull. seism. Soc. Am.*, **93**, 1012–1033.
- Cauzzi, C., Faccioli, E., Vanini, M. & Bianchini, A., 2015. Updated predictive equations for broadband (0.01–10 S) horizontal response spectra and peak ground motions, based on a global dataset of digital acceleration records, *Bull. Earthq. Eng.*, **13**, 1587–1612.
- Comité Européen de Normalisation (CEN) (2004). Eurocode 8, design of structures for earthquake resistance part 1: general rules, seismic actions and rules for buildings. European Standard EN 1998–1, Brussels.
- Chiou, B., Darragh, R., Gregor, N. & Silva, W., 2008. Nga project strong-motion database, *Earthq. Spectra*, **24**, 23–44.
- Chiou, B.S.-J. & Youngs, R.R., 2008. An Nga model for the average horizontal component of peak ground motion and response spectra, *Earthq. Spectra*, **24**, 173–215.
- Chiou, B.S.-J. & Youngs, R.R., 2014. Update of the Chiou and Youngs Nga model for the average horizontal component of peak ground motion and response spectra, *Earthq. Spectra*, **30**, 1117–1153.
- Delavaud, E. *et al.*, 2012a. Toward a Ground-Motion Logic Tree for Probabilistic Seismic Hazard Assessment in Europe, *J. Seismol.*, **16**, 451–473.
- Delavaud, E., Scherbaum, F., Kuehn, N. & Allen, T., 2012b. Testing the global applicability of ground-motion prediction equations for active shallow crustal regions, *Bull. seism. Soc. Am.*, **102**, 707–721.
- Douglas, J. & Boore, D.M., 2011. High-frequency filtering of strong-motion records, *Bull. Earthq. Eng.*, **9**, 395–409.
- Douglas, J. & Edwards, B., 2016. Recent and future developments in earthquake ground motion estimation, *Earth-Sci. Rev.*, **160**, 203–219.
- Douglas, J. *et al.*, 2014. Comparisons among the five ground-motion models developed using resource for the prediction of response spectral accelerations due to earthquakes in Europe and the Middle East, *Bull. Earthq. Eng.*, **12**, 341–358.
- Drouet, S. & Cotton, F., 2015. Regional stochastic gmpes in low-seismicity areas: scaling and aleatory variability analysis—application to the French Alps, *Bull. seism. Soc. Am.*, **105**, 1883–1902.
- Drouet, S., Bouin, M.-P. & Cotton, F., 2011. New moment magnitude scale, evidence of stress drop magnitude scaling and stochastic ground motion model for the French West Indies, *Geophys. J. Int.*, **187**, 1625–1644.
- Edwards, B. & Fäh, D., 2013. A stochastic ground-motion model for Switzerland, *Bull. seism. Soc. Am.*, **103**, 78–98.
- Edwards, B., Rietbrock, A., Bommer, J.J. & Baptie, B., 2008. The acquisition of source, path, and site effects from microearthquake recordings using Q tomography: application to the United Kingdom, *Bull. seism. Soc. Am.*, **98**, 1915–1935.
- Edwards, B., Poggi, V. & D. Fäh, 2011. A predictive equation for the vertical-to-horizontal ratio of ground motion at rock sites based on shear-wave velocity profiles from Japan and Switzerland, *Bull. seism. Soc. Am.*, **101**, 2998–3019.
- Edwards, B., Michel, C., Poggi, V. & D. Fäh, 2013. Determination of site amplification from regional seismicity: application to the swiss national seismic networks, *Seismol. Res. Lett.*, **84**, 611–621.
- Edwards, B., Cauzzi, C., Danciu, L. & Fäh, D., 2016. Region-specific assessment, adjustment and weighting of ground motion prediction models: application to the 2015 swiss seismic hazard maps, *Bull. seism. Soc. Am.*, **106**.
- Hashash, Y.M. *et al.*, 2014. Reference rock site condition for central and Eastern North America, *Bull. seism. Soc. Am.*, **104**, 684–701.
- Joyner, W.B., Warrick, R.E. & Fumal, T.E., 1981. The effect of quaternary alluvium on strong ground motion in the Coyote Lake, California, Earthquake of 1979, *Bull. seism. Soc. Am.*, **71**, 1333–1349.
- Kottke, A.R. & Rathje, E.M., 2008. *Technical Manual for Strata*, University of California.
- Laurendeau, A., Cotton, F., Ktenidou, O.J., Bonilla, L.F. & Hollender, F., 2013. Rock and stiff-soil site amplification: dependency on V-S30 and Kappa (Kappa(0)), *Bull. seism. Soc. Am.*, **103**, 3131–3148.
- McGuire, R.K., 2008. Probabilistic seismic hazard analysis: early history, *Earthq. Eng. Struct. Dyn.*, **37**, 329–338.
- Michel, C., Edwards, B., Poggi, V., Burjanek, J., Roten, D., Cauzzi, C. & Fäh, D., 2014. Assessment of site effects in alpine regions through systematic site characterization of seismic stations, *Bull. seism. Soc. Am.*, **104**, doi:10.1785/0120140097.
- Molas, G.L. & Yamazaki, F., 1995. Attenuation of earthquake ground motion in Japan including deep-focus events, *Bull. seism. Soc. Am.*, **85**, 1343–1358.
- Motazedian, D. & Atkinson, G.M., 2005. Stochastic finite-fault modeling based on a dynamic corner frequency, *Bull. seism. Soc. Am.*, **95**, 995–1010.
- Nigam, N.C. & Jennings, P.C., 1969. Calculation of response spectra from strong-motion earthquake records, *Bull. seism. Soc. Am.*, **59**, 909–922.
- Pagani, M. *et al.*, 2014. Open quake engine: an open hazard (and Risk) software for the global Earthquake Model, *Seismol. Res. Lett.*, **85**, 692–702.
- Poggi, V., Edwards, B. & Fäh, D., 2011. Derivation of a reference shear-wave velocity model from empirical site amplification, *Bull. seism. Soc. Am.*, **101**, 258–274.
- Poggi, V., Edwards, B. & Fäh, D., 2012. Characterizing the vertical-to-horizontal ratio of ground motion at soft-sediment sites, *Bull. seism. Soc. Am.*, **102**, 2741–2756.
- Poggi, V., Edwards, B. & Fäh, D., 2013. Reference S-wave velocity profile and attenuation models for ground-motion prediction equations: application to Japan, *Bull. seism. Soc. Am.*, **103**, 2645–2656.
- Poggi, V., Edwards, B. & Fäh, D., 2017. A comparative analysis of site-specific response spectral amplification models, *Phys. Chem. Earth Parts A/B/C*, **98**, 16–26.

- Renault, P., 2014. Approach and challenges for the seismic hazard assessment of nuclear power plants: the swiss experience, *Boll. Geofis. Teor. Appl.*, **55**, 149–164.
- Rodriguez-Marek, A., Montalva, G.A., Cotton, F. & Bonilla, F., 2011. Analysis of single-station standard deviation using the Kik-net data, *Bull. seism. Soc. Am.*, **101**, 1242–1258.
- Scherbaum, F., Schmedes, J. & Cotton, F., 2004. On the conversion of source-to-site distance measures for extended earthquake source models, *Bull. seism. Soc. Am.*, **94**, 1053–1069.
- Scherbaum, F., Cotton, F. & Staedtke, H., 2006. The estimation of minimum-misfit stochastic models from empirical ground-motion prediction equations, *Bull. seism. Soc. Am.*, **96**, 427–445.
- Scherbaum, F., Delavaud, E. & Riggelsen, C., 2009. Model selection in seismic hazard analysis: an information-theoretic perspective, *Bull. seism. Soc. Am.*, **99**, 3234–3247.
- Wells, D.L. & Coppersmith, K.J., 1994. New empirical relationships among magnitude, rupture length, rupture width, rupture area, and surface displacement, *Bull. seism. Soc. Am.*, **84**, 974–1002.
- Zhao, J.X. & Lu, M., 2011. Magnitude-scaling rate in ground-motion prediction equations for response spectra from large, shallow crustal earthquakes, *Bull. seism. Soc. Am.*, **101**, 2643–2661.
- Zhao, J.X. *et al.*, 2006. Attenuation relations of strong ground motion in Japan using site classification based on predominant period, *Bull. seism. Soc. Am.*, **96**, 898–913.

SUPPORTING INFORMATION

Supplementary data are available at [GJI](#) online.

Electronic Appendix.xlsx

Please note: Oxford University Press is not responsible for the content or functionality of any supporting materials supplied by the authors. Any queries (other than missing material) should be directed to the corresponding author for the paper.